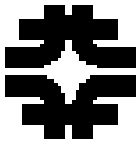

11/10/2013
TD-13-013

Study of the quench propagation in the high-field superconducting quadrupoles for the LHC luminosity upgrade

Vittorio Marinozzi

Abstract

In 2022 the Large Hadron Collider at CERN is expected to undergo a significant upgrade in order to increase its luminosity. A major role will be played by the new, more performing superconducting quadrupoles that will be set in the interaction zones. The goal of this thesis is to study the quench protection of these magnets (MQXF). MQXF is an eight-meters long Nb_3Sn superconducting magnet, with a very large aperture (150 mm). At the nominal current (17.3 kA), its stored energy is 12.2 MJ, therefore the quench protection is challenging. Two codes have been used for this study: QLASA, developed by INFN-LASA and University of Milan, and ROXIE, developed by CERN. Past experience using these codes on Nb_3Sn magnets is very limited, and they need to be validated for application using this superconductor. Therefore, a previously started work aiming at validating these codes with experimental data from the US-LARP collaboration has been completed, and the results are reported here. Subsequently, the validated models have been used for predicting the MQXF hot spot temperature during a quench, and the results are reported and discussed. The conclusion of this preliminary work is that, under the conservative assumptions used so far, the MQXF protection seems quite challenging. Nonetheless, more realistic assumptions should increase the protection margin. An improvement of this study aiming at more realistic assumptions is in progress.

Fermi National Accelerator Laboratory / Kirk Road and Pine Street / P.O. Box 500 / Batavia, IL 60510 / 630.840.3000 / www.fnal.gov / fermilab@fnal.gov
Office of Science / U.S. Department of Energy / Managed by Fermi Research Alliance, LLC

Fermi National Accelerator Laboratory / Kirk Road and Pine Street / P.O. Box 500 / Batavia, IL 60510 / 630.840.3000 / www.fnal.gov / fermilab@fnal.gov

Office of Science / U.S. Department of Energy / Managed by Fermi Research Alliance, LLC

Facoltà di Scienze Matematiche Fisiche e Naturali

Corso di Laurea Magistrale in Fisica

Study of the quench propagation in the high-field superconducting quadrupoles for the LHC luminosity upgrade

Relatore interno: Dr. SORBI Massimo

Relatore esterno: Dr. AMBROSIO Giorgio

Correlatore: Ing. MANFREDA Giulio

Tesi di laurea di:
MARINOZZI Vittorio
Matr. 791623

Anno Accademico 2012-2013

Contents

Chapter 1

Particle accelerators and magnetic quadrupoles

1.1 Introduction

Particle accelerators are machines designed for increasing the energy of charged particles. The simplest accelerator is constituted by a simple static voltage difference, for example between two charged metallic planes. A particle gains an energy equal to $\Delta E = q\Delta V$, where ΔV indicates the voltage difference, when it passes through the gap.
One of the main applications of the accelerators is the nuclear and particle physics research. In this context, very high energy values are required (LHC will reach 7 TeV per beam!), therefore an electrostatic accelerator, as that described before, is surely unsuitable, because it can reach energy of only few keV. So, research accelerators are complex machines, and their main feature is that particles are accelerated many times by the same voltage difference.
In the electrostatic case, in absence of sources, the well-known equation 1.1 is valid

$$\vec{\nabla} \times \vec{E} = 0 \tag{1.1}$$

or, in integral form

$$\oint \vec{E} \cdot \vec{dl} = 0 \tag{1.2}$$

So, if the particle had returned at the entrance of the voltage difference gap, its energy was necessarily that possessed before the acceleration! In fact, the electrostatic field is conservative.
Instead, it's possible to use the same voltage difference in order to accelerate a charged particle several times by means of time variant electromagnetic fields. You can see in the fig. 1.1 that, if you reverse the charged planes polarity during the gap crossing time, the particle is accelerated again, and it gains an energy equal to $\Delta E = q\Delta V$ in every gap. This simply describes

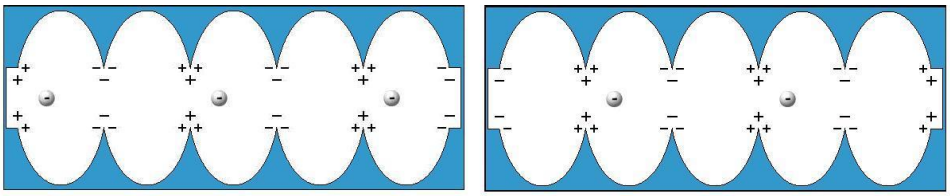

Figure 1.1: Particle acceleration by means of time variant fields

the acceleration process in the *resonant cavities*, where charged particles are accelerated by an electromagnetic traveling wave that resonates in the cavity.
Accelerators can be distinct in two main groups:

- Linear accelerators (LinAc): in these machines, particles go through a huge number of resonant cavities set on a straight line. In this way particles can reach the highest energy in the minor possible space. Generally, these machines are used as injector for circular machines, regarding to protons or heavy-ions (you can easily understand that in a LinAc the initial particles energy can be zero, while in a circular accelerator particles need a positive initial energy), instead they are more suitable for the high energy acceleration of light particles like electrons, because in the circular machines their acceleration is limited by the radiation emission.

- Circular accelerators: in these machines, particles are held on a circular orbit by dipolar magnetic fields, because of the Lorentz force

$$\vec{F} = q\vec{v} \times \vec{B} \tag{1.3}$$

  At every turn, particles go through one or more resonant cavities: it's so possible to reach very high energy by means of a huge number of turns, even if the energy gain per turn is not high. Circular accelerators examples are the cyclotron (fixed magnetic field, variable orbit) or the synchrotron (fixed orbit, variable magnetic field). The latter is often used in physics as *collider*: two particle beams circulate in opposite direction and collide in some specific points of the accelerator; results of these collisions (called *events*) are collected and elaborated by appropriate detectors. We will see in the section 1.2 that the quadrupolar magnets have a primary role in these machines.
  The circular accelerators limit is that the bigger the designed particle energy is, the bigger the accelerator size: in fact, in addition to the radiation emission, you have to consider the maximum magnetic field that dipoles can reach in order to bend the beam. You can easily prove that, for a charged particle in motion inside an uniform magnetic field,

eq. 1.4 is valid

$$\frac{p}{q} = B\rho \tag{1.4}$$

where ρ is the orbit radius, B the magnetic field, and p the particle momentum; you can see that, if you want to improve the particle energy, and so to improve the momentum, at the maximum magnetic field you must increase the orbit radius, and so the machine size. The product $B\rho$ is called beam *rigidity*: the bigger the rigidity is, more difficult is bending the beam by means of magnetic fields . LHC, the accelerator with the highest beam energy, has a circumference of 27 km! In order to reduce the machines size, modern synchrotrons are provided of superconductive dipoles, able to generate higher magnetic fields with reduced expenses.

1.2 Beam focusing

Consider the free space propagation on a tract of length L of a particle in initial position x_0 and with divergence $\dot{x}$ (see the fig. 1.2), where $\dot{x}$ indicates the derivative respect to s. The final particle position is

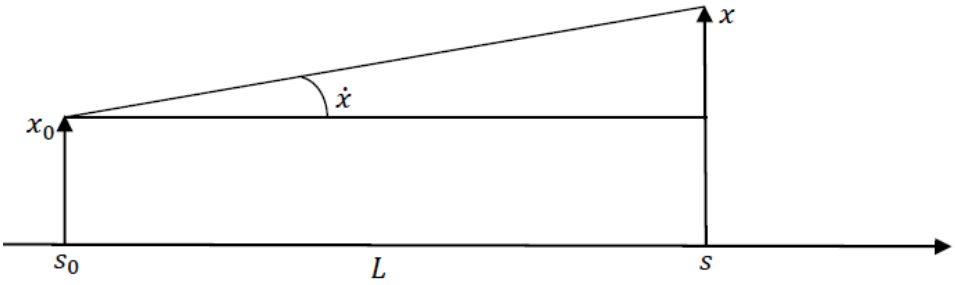

Figure 1.2: Particle propagation on free space

$$x = x_0 + L\tan\dot{x} \simeq x_0 + L\dot{x} \tag{1.5}$$

while the divergence is constant. Therefore you can write, in matrix form

$$\begin{pmatrix} x \\ \dot{x} \end{pmatrix} = \begin{pmatrix} 1 & L \\ 0 & 1 \end{pmatrix} \begin{pmatrix} x_0 \\ \dot{x}_0 \end{pmatrix} \tag{1.6}$$

Generally, it's always possible to describe the motion of a particle in a linear system (and an accelerator is a linear system, at the first order) by means of the equation

$$\vec{x} = M\vec{x}_0 \tag{1.7}$$

where $\vec{x}$ and $\vec{x}_0$ are the particle coordinates respectively at the begin and at the end of the system, and M is called the *transport matrix* of the system.

1.2.1 Transport matrix of a magnetic quadrupole

Let's try to find the transport matrix of a magnetic quadrupole. The reference system moves together with the reference particle (the ideal particle that is on a perfect circular orbit in the bending sections, on a perfect straight trajectory in the focusing sections), as you can see in the fig. 1.3. A perfect quadrupolar field is represented by

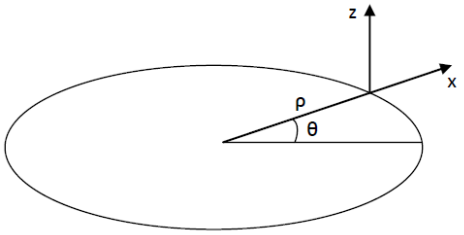

Figure 1.3: Reference system for beam particles. The reference particle is on the origin of the system

$$\begin{cases} B_x = Gz \\ B_z = Gx \\ B_s = 0 \end{cases} \tag{1.8}$$

where the longitudinal coordinate is $s = \rho\theta$. For a particle with charge q in such a field, and in absence of acceleration, the motion equations are

$$\begin{cases} m\frac{d^2x}{dt^2} = q(v_s B_z - v_z B_s) \\ m\frac{d^2z}{dt^2} = q(v_x B_s - v_s B_x) \\ m\frac{d^2s}{dt^2} = q(v_z B_x - v_x B_z) \end{cases} \tag{1.9}$$

We can assume that the velocity has only longitudinal component, i.e. $v \simeq v_s$, and, by replacing eq. 1.8 in eq. 1.9, we obtain

$$\begin{cases} m\frac{d^2x}{dt^2} = qvGx \\ m\frac{d^2z}{dt^2} = -qvGz \\ m\frac{d^2s}{dt^2} = 0 \end{cases} \tag{1.10}$$

The longitudinal motion is simply uniform rectilinear, so we pay attention only on the transversal motion. By doing the variable change $s = vt$, eq. 1.10 become

$$\begin{cases} \ddot{x} = \frac{qG}{mv}x \\ \ddot{z} = -\frac{qG}{mv}z \end{cases} \tag{1.11}$$

The product mv is the particle momentum, therefore by replacing eq. 1.4 in eq. 1.11 we obtain

$$\begin{cases} \ddot{x} = \frac{G}{B\rho} x \\ \\ \ddot{z} = -\frac{G}{B\rho} z \end{cases} \tag{1.12}$$

Assuming $G > 0$, we can see that the quadrupolar field has a focusing effect on the axial plane (it's the harmonic motion equation!), while it has a defocusing effect on the radial plane. You can note that the focusing power is directly proportional to the field gradient, and inversely proportional to the beam rigidity. Therefore, you can describe the motion of a particle that goes through a quadrupole with length L, with initial coordinates x_0 and $\dot{x}_0$, by solving the differential equations 1.12. The solutions are well known, and in matrix form they are:

$$\begin{pmatrix} x \\ \dot{x} \end{pmatrix} = \begin{pmatrix} \cosh kL & \frac{1}{k}\sinh kL \\ k\sinh kL & \cosh kL \end{pmatrix} \begin{pmatrix} x_0 \\ \dot{x}_0 \end{pmatrix} \tag{1.13}$$

$$\begin{pmatrix} z \\ \dot{z} \end{pmatrix} = \begin{pmatrix} \cos kL & \frac{1}{k}\sin kL \\ -k\sin kL & \cos kL \end{pmatrix} \begin{pmatrix} z_0 \\ \dot{z}_0 \end{pmatrix} \tag{1.14}$$

where

$$k^2 = \frac{G}{B\rho} \tag{1.15}$$

The matrices structure is similar, but in the focusing case you have trigonometric functions, in the defocusing case you have hyperbolic functions.

1.2.2 Beam motion

The motion of a beam is more complicated than that of a single particle; for details, you can refer to [2]. Briefly, a beam is described by an ellipse in the phase space ($\vec{x}$,$\vec{\dot{x}}$). The ellipse evolution represents the beam behavior under the effect of the machine components.
A synchrotron is a periodic machine (at least, the period is the whole circumference). You can prove that the beam motion has the same periodicity of the machine. Therefore, you can reach beam focusing by repeating several times a small system with a focusing effect on the beam. The simplest system of this kind is the *FODO cell*: it is composed by a focusing quadrupole (F), a free space (O), a defocusing quadrupole (D) and another free space. You can prove that such a system has a focusing effect on both radial and axial direction, under some conditions. In some of the free spaces dipoles are inserted, in order to bend the beam; focusing effect from dipoles is negligible, so the periodicity is preserved.
FODO is only one of the focusing system that has been studied: different configurations of focusing and defocusing quadrupoles are used in order to

focus the beam. In particular, in the colliders intersection zone, called *low β insertion*, a particular configuration is used.

1.2.3 Insertions

One of the most important parameters characterizing the colliders is the ***luminosity***. This quantity is proportional to the rate of events when a collision occurs in the interaction point. Clearly, the smaller the beam cross section is, the bigger the luminosity. Therefore, one of the ways suitable to improve luminosity is reducing the beam transversal size by means of a strong focusing quadrupoles configuration. These are very long sequences of focusing and defocusing quadrupoles, and in the interaction zone the beam radial and transversal sizes are very small.
The quadrupoles focusing power is related to the magnetic field and to the gradient that they can reach. We are going to see that superconducting quadrupoles can generate much stronger fields than resistive ones, so they are useful in order to reach very high luminosity level.

1.3 Magnetic design for a quadrupole

Resistive quadrupoles are built by winding copper cables around iron poles. Because of cables resistivity, current contribute to the magnetic field is negligible respect to the iron one. Therefore, the magnetic field quality is strongly related to the iron poles shape.
From the equation 1.8, it's clear that the scalar potential

$$\phi(x, z) = Gxz \tag{1.16}$$

generates a perfect quadrupolar field. In the case of no-saturated iron, the poles surfaces are equipotential surfaces, so if we put

$$\phi(x, z) = \pm constant \tag{1.17}$$

we find that hyperbolic iron poles generate a quadrupolar field. It's clear that the iron shape cannot be perfect, so the field is never perfectly quadrupolar.
In the resistive case, the focusing power is limited by the iron saturation: iron cannot generate magnetic field higher than about 2 T. It's possible to improve it by increasing the flowing current, but this process is limited by cables heating and size. Superconducting quadrupoles have been developed in order to overcome this obstacle.

As we are going to see in the chapter 2, the main superconductors feature is that they can carry very high current without generating heat, so they can generate magnetic fields very higher than iron can do: in the superconducting quadrupoles the field intensity and quality is related to the

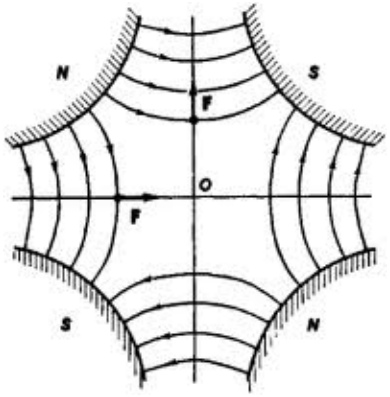

Figure 1.4: Iron shape for an ideal resistive quadrupole

current and to the cables design; generally, iron is not used for poles, but for mechanical reasons and for closing the magnetic field lines.
It's so clear that the superconducting windings design is very important in order to develop a good magnet. You can prove that a perfect quadrupolar field is generated by a surface current distribution as

$$J_z = J_0 \cos 2\theta \tag{1.18}$$

Obviously, such a current distribution is impossible to obtain, so windings

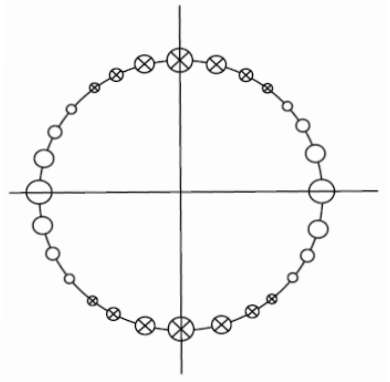

Figure 1.5: Current distribution that generates a quadrupolar field. Axis z is perpendicular to the page

are designed in order to be as similar as possible to a $\cos 2\theta$ current distribution. Fig. 1.6 represents examples of cross section design for superconducting quadrupoles.

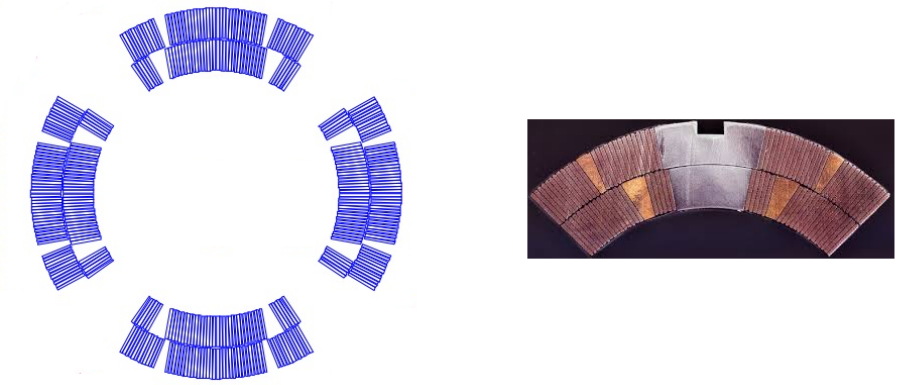

Figure 1.6: On the left, the cross section design for the MQXF quadrupole. On the right, a quarter of the HQ quadrupole real windings

1.4 HiLumi

LHC is now the most powerful collider of the world: two beams of protons circulate in opposite directions with an energy of 3.5 TeV per beam (in the 2015, 7 TeV per beam will be reached) and collide in four interaction points, where apposite detectors collect the data. Luminosity is a very important parameter, because if you have a high luminosity, each event produces a higher number of useful data, so you can reach your results faster. That's why CERN is developing a project called ***HiLumi*** in order to improve the LHC luminosity in the 2020 about.
In this project, the new superconducting quadrupoles for the low β insertions play a very important role: luminosity increase is related to the beams transversal size reduction, so new more performing superconducting quadrupoles are under development.
MQXF is one of the low β quadrupoles proposed for the LHC luminosity upgrade. It's a 8 m long quadrupole, with an aperture of 150 mm, a peak field of 12.2 T and a gradient of 140 T/m. The purpose of this thesis work is to analyze the quench propagation in the MQXF, and to describe the quench protection needed for it. Quench is the process in which the superconductors become resistive, and it's described in details in the chapter 2.

Chapter 2

Quench and protection

2.1 Superconductivity signs

The superconductivity is a special matter state, and it has been discovered in the 1911 by the Dutch physicist Heike Kamerlingh Onnes. By reducing the temperature of mercury samples under a certain threshold, he noted that they showed null electric resistivity. Later, it was discovered that this phenomenon was accompanied by the magnetic field expulsion (*Meissner effect*). Superconducting properties have lots of applications, (for example, Meissner effect is used to build magnetic levitation trains), but we are mostly interested in applications on particle accelerator development. In particular, it's possible to develop high field magnets by making use of superconducting materials, because they have null electrical resistivity, so very high currents can flow through them without generating heat. Therefore, you can get very high field at costs lower than with standard magnets.
We have already said that a superconducting material has to be under a certain temperature, called *critical temperature*, in order to maintain superconducting properties. In reality, this temperature also depends on the density current that flows in the material, and on the magnetic field at which the material is subjected; in practice, in order to maintain superconducting properties, a material has to be in a zone delimitated by a so called *critical surface*, as you can see in the fig. 2.1. Interceptions with the three axes are called *critical temperature* T_c, *critical field* H_c and *critical current* J_c. You can note that on the critical surface, when you augment one quantity, both the others decrease.
It's so clear that, if you want to use superconductors, you must maintain these parameters under their critical values; obviously, critical values vary in dependence of the chosen material.

All these considerations are valid for materials so called *type-I superconductors*; there is another class of superconductors, called *type-II superconductors*, that have two critical values for the magnetic field: under the first

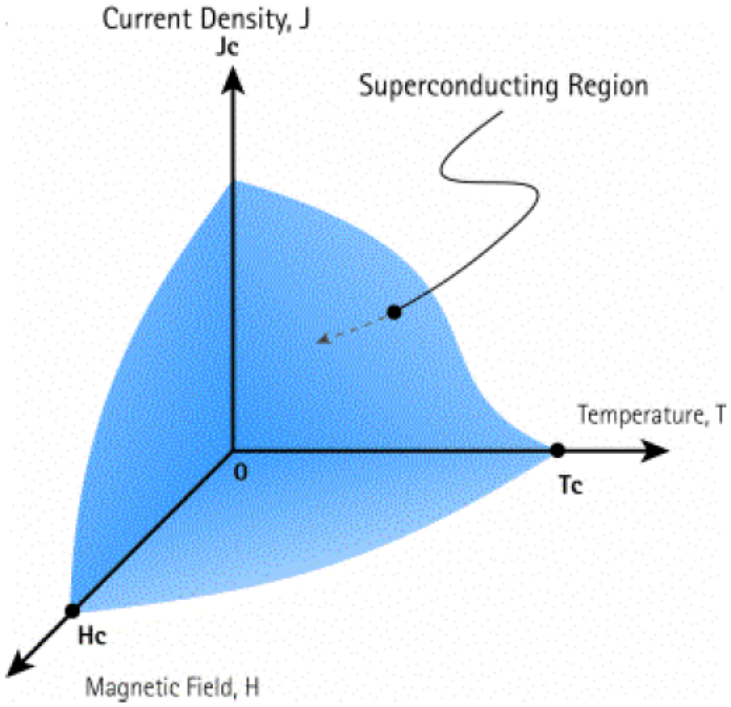

Figure 2.1: Critical surface example: a material maintain his superconducting properties under it

Critical values $NbTi$		
T_c	H_{c1}	H_{c2}
9.4 K	$0.3 - 1$ Oe	$120 - 150$ kOe

Table 2.1: Critical values for $NbTi$

of them, material is like a normal type-I superconductor; between the first and the second, magnetic field can partially penetrate inside the material, but superconducting features are held; beyond the second, the material loses superconducting properties. Type-II superconductors are so used in magnets building, because generally they can reach magnetic fields higher than type-I superconductors can do.
Till now, $NbTi$ (*niobium-titanium*) has been the most utilized type-II superconductor in accelerator magnets. Critical parameters[11] are reported in the tab. 2.1. $NbTi$ can so be utilized as superconductor if cooled with helium at a temperature of 1.9 K (superfluid helium temperature). $NbTi$ has great mechanical properties, similar to those of a simple metal.
$NbTi$ has almost reached his highest performances, so, in the last years, the study of another superconducting material, the Nb_3Sn (*niobium-three-tin*),

Critical values Nb_3Sn		
T_c	H_{c1}	H_{c2}
18 K	$0.2 - 0.4$ kOe	$220 - 250$ kOe

Table 2.2: Critical values for Nb_3Sn

has been carried on, because this material has more performance features, as you can see[11] in the tab. 2.2. However, Nb_3Sn has mechanical properties more similar to those of ceramics than to those of metals, so the realization of windings is very difficult; moreover, protection systems of Nb_3Sn magnets have to be more efficient, and we will see the reasons in the section 2.3.

2.2 Causes of quench

We have already seen that a material has to be under the critical surface in order to maintain its superconducting properties. When one of the three parameters (temperature, field or current) exceeds its critical value, the material leaves the superconductive state and it returns in the normal state: this phenomenon is called **quench**. Clearly, its consequences could be destructive for an accelerator magnet, because currents of tens kA suddenly flow in cables with bad electrical and thermal features (superconductors are usually bad conductors in the normal state): so, in case of quench, normal zones have to dissipate in heat all the stored energy $\frac{1}{2}LI^2$, and there is risk of melting cables. Quench study is so very important in the superconducting magnets design.
Let's see now the possible causes of quench.

2.2.1 Degradation and training

We have already seen that superconductors can carry a maximum current J_c, over whom a quench occurs, despite they have null electrical resistivity. Critical current can be measured on short cable samples. But when you make windings with cables, coils never reach the performances measured on the short sample, and a quench occurs at current minor than nominal critical current: this phenomenon is called *degradation*. It can be caused by the defects and micro-breakages that occur in cables when they are wound, but today the winding techniques are good enough to prevent them, so the main causes are mechanical stresses. Near degradation, a magnet is always subjected to another phenomenon called *training*: suppose that we ignite a magnet for the first time, and a quench occurs at say 50% of nominal critical current; at the subsequent ignition the magnet will reach a major percentage of the critical current, say 60%, and later a major percentage again, until to settle on a stable percentage (nominal critical current is never

Time	Space	
	Point	Distributed
Transient	J	J/m^3
Continuous	W	W/m^3

Table 2.3: Disturbance spectrum

reached, because of the degradation). A good magnet reach stable zone in few cycles of cooling-warming, and it reaches at least 85% of the nominal critical current. The training is mainly due to the coils movements under the action of the strong electromagnetic forces that act on windings: the friction between coils can deliver enough energy to start a quench process. At the subsequent ignition, however, the coil in which quench started is in equilibrium position, so the current can increase until another coil moves, or until critical current is reached.

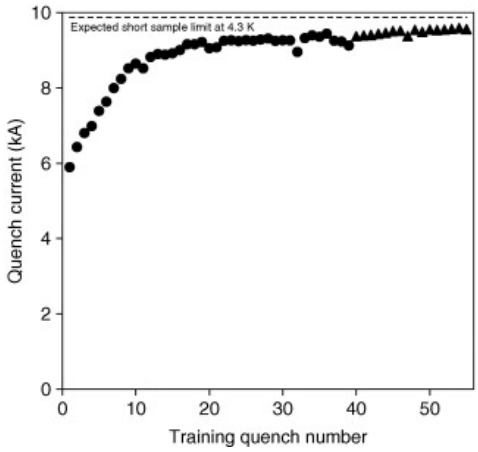

Figure 2.2: Training and degradation example

2.2.2 The disturbance spectrum

Generally, you can say that every quench event is due to an energy release within the coils, as the field and the current are increased. Temperature locally rises because of this energy, so the critical current is reduced and if it goes under the current that flows in the magnet, heat is produced and a quench could occur. It's so important to know the amount of energy needed to start a quench. It's useful to introduce the *disturbance spectrum*, which encompasses all the energy disturbances that could occur within a superconducting magnet winding. Continuous disturbance are caused by steady power input, that could be due, for example, to a bad joint (point distur-

bance), or to excessive a.c. and magnetization hysteresis losses (distributed disturbance). Continuous disturbance are so well known and they don't produce training, but only degradation. They generally don't cause serious problems.
Transient disturbance are instead the dominant cause of degradation in magnets, and they may cause serious problems. A type of transient disturbance is the *flux jumping*, that is a natural instability of superconducting materials under current variation. This effect can be reduced by decreasing superconducting filaments size, so today it's not a big problem. The mechanical movements are another problem, and they are responsible of the training behavior. It's impossible to predict and prevent all of them.

In the next sections we will calculate relationships between quenching current and disturbance size, in order to predict the minimum energy release that can origin a quench, and the temperature rise of the zone in which quench starts.

2.2.3 Distributed disturbances

If an energy release occurs in a big zone of the windings, its temperature raise will be determined only by its heat capacity

$$\partial T = \frac{\partial Q}{C} \tag{2.1}$$

At very low temperature, heat capacity strongly depends on the temperature, so it's convenient to talk in terms of enthalpy $H(T) = \int_0^T C(T)\, dT$. Some enthalpy plot examples are reported in fig. 2.3.

Suppose that the critical current linearly depends on the temperature, as shown in fig. 2.4. If T_0 is the coolant temperature, it's clear that if the corresponding critical current J_{co} flows in the cables, the lowest release of energy will develop a quench, because temperature rise makes the current higher than critical current, and critical current always falls with temperature. For this reason, as margin of safety, a sub-critical current J_M flows in the conductors. You can see in fig. 2.4 that the temperature at which the heat generation starts is given by

$$T_g = T_c - (T_c - T_0)\frac{J_M}{J_{c0}} \tag{2.2}$$

You can use equation 2.2 and data from "typical winding" in fig. 2.3 in order to estimate the energy needed to reach T_g. For example, an energy of only 750 J/m^3 is needed to reach T_g at the 90% of the nominal critical current with helium temperature $T_0 = 4.2$ K; this is a very small release of energy, that would raise the windings temperature by only 10^{-4} K at room temperature.

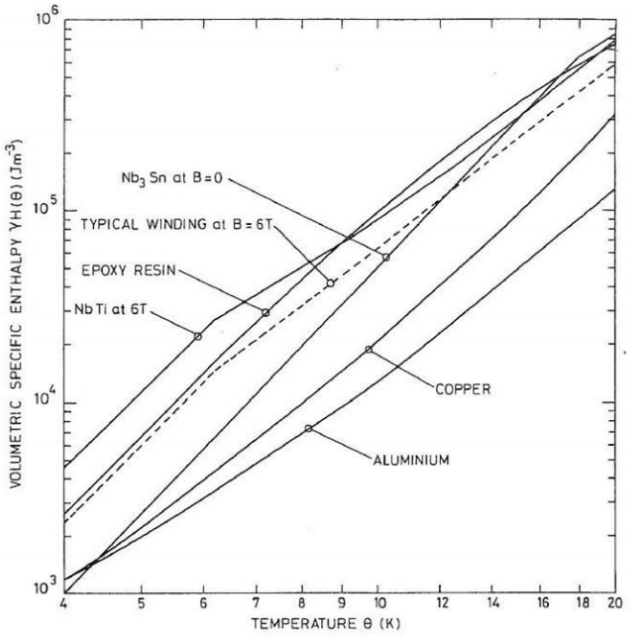

Figure 2.3: Some enthalpy plots for different materials

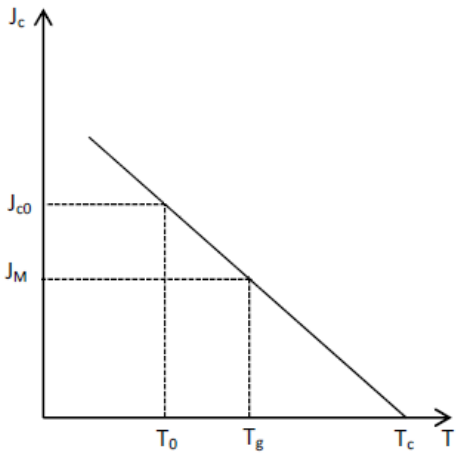

Figure 2.4: Critical current as function of the temperature

2.2.4 Point disturbances and MPZ

Consider a hot spot at temperature T_c. This spot is normal, and it generates a heat power equal to $J_c^2 \rho A l$, where ρ is the normal state resistivity, A the cross-section area of the wire, and l the normal zone length. Under balance, the power generated is equal to that conduced along the wire, according to

the Fourier equation

$$\frac{P}{A} = -k\frac{\partial T}{\partial x} \tag{2.3}$$

where k is the longitudinal heat conductivity. We can assume that the temperature rise is linear, so equation 2.3 becomes

$$J_c^2 \rho A l = 2kA\frac{(T_c - T_0)}{l} \tag{2.4}$$

and so

$$l = \left[\frac{2k(T_c - T_0)}{J_c^2 \rho}\right]^{\frac{1}{2}} \tag{2.5}$$

A normal zone longer than l will grow, because heat generation hangs

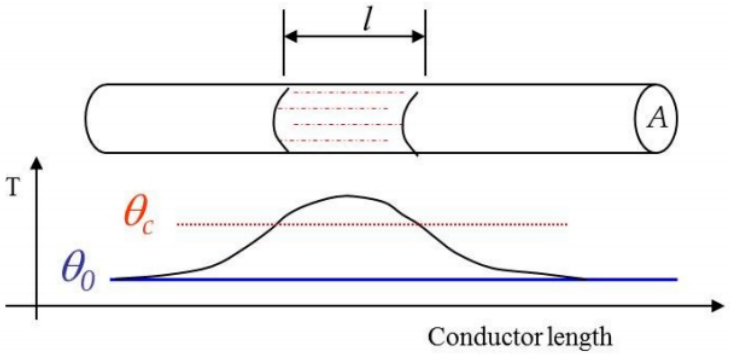

Figure 2.5: MPZ for an uniform wire

over heat conduction; otherwise, a normal zone smaller than l will collapse and superconductivity is restored. For these reasons, l is called *Minimum Propagating Zone* (MPZ). Energy needed in order to establish the MPZ is very small: for example, in a $NbTi$ wire of 0.3 mm diameter cooled with boiling helium ($T_0 = 4.2K$) MPZ is only 0.5 μm and the energy needed to establish it is only 10^{-9} J. So, wire composed of only superconductor cannot be used, because they are vulnerable to the slightest disturbance. Composite conductors have been developed in order to improve magnets performances.

2.2.5 Composite conductors

Modern superconducting wires have a complex cross-sectional structure. Generally, very thin superconducting filaments of $\sim$ 10 μm diameter are organized in a copper matrix. Sometimes, a copper nucleus protected by a tantalum barrier is present. Fig. 2.6 reports some superconducting wires examples. Presence of copper augments the conductivity and the heat capacity, and it reduces the resistivity, therefore these wires are more resistant to disturbances.

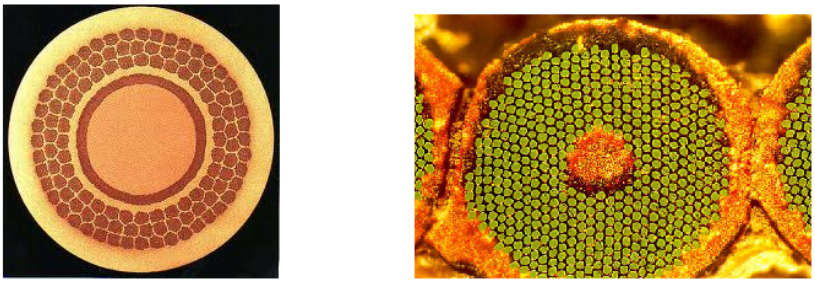

Figure 2.6: Cross section of modern superconductors. On the left you can see the tantalum barrier

Clearly, a one-dimension calculation for the MPZ as in the section 2.2.4 is not suitable, because the wire is very anisotropic. A three-dimension calculation can be carried on, and for the details you can refer to [1]. The result is that the MPZ is an ellipsoid, as shown in fig. 2.7, elongated in the z-direction, parallel to the wire. This shape is due to the fact that in the

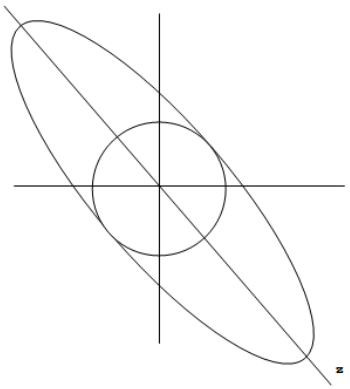

Figure 2.7: MPZ for a composite wire

longitudinal direction copper heat conductivity is dominant, in the transversal direction superconductor heat conductivity is dominant.
These kind of wires needs higher energy release in order to establish MPZ, of the order of $\sim 10^{-5}$ J, but this energy is very small too, so quench can always occur and magnets always need a suitable quench protection.

2.3 Quench propagation

When a quench occurs, accelerator magnets have to dissipate in heat a very high energy $\frac{1}{2}LI^2$, because they generally have high inductance, and they carry high current. In the section 2.2 we've seen that generally quench is caused by point disturbances. If the quench propagation is slow, all the energy is dissipated in a very little zone, and its temperature could rise until damaging the magnet. To prevent this situation, it's important to study the temperature rise of the normal zone and the quench propagation velocity.

2.3.1 Temperature rise and MIITs

During a quench the normal zone expands with time because of the heat conduction. Clearly, the zone in which the quench starts has the highest temperature, so we will call it the *hot spot*. In order to protect the magnet, it's important to maintain the hot spot temperature under a suitable level. For the calculation of the hot spot temperature, we can assume local adiabaticity; obviously this is a tricky approximation, because quench couldn't propagate, but the error is conservative, so we can accept it.
If we assume local adiabaticity, all the energy per volume unit is absorbed by the specific heat

$$J^2(t)\rho(T)dt = \gamma C(T)dT \tag{2.6}$$

where ρ is the resistivity, γ the density and C the specific heat. Multiplying for the square section area of the wire, dividing for the resistivity and integrating we obtain

$$\int_0^t I^2(t)\,dt = A^2 \int_{T_0}^{T} \frac{\gamma C(T)}{\rho(T)}\,dT \tag{2.7}$$

Dividing the integral on the right in the equation 2.7 by 10^6, we obtain an important quantity called **MIITs**.

$$\mathrm{MIITs}(T) = A^2 \int_{T_0}^{T} \frac{\gamma C(T)}{10^6\rho(T)}\,dT \tag{2.8}$$

The name MIITs is due to the measure unit, that is $\mathrm{MA}^2\mathrm{s}$. This quantity is very important because it depends only on the material properties and on the section of the wire. If we know them, we can plot the MIITs vs temperature function. Then, if we know the $I^2(t)$ function, we can integrate it, calculate the MIITs developed, and find on the MIITs plot the temperature that the hot spot has reached. For example, consider the ciruit in the fig. 2.8. The magnet is represented by its inductance, and there is an external resistance R. We are neglecting the resistance developed by the quench. Clearly, the starting current I decays according to the equation

$$I(t) = Ie^{-\frac{Rt}{L}} \tag{2.9}$$

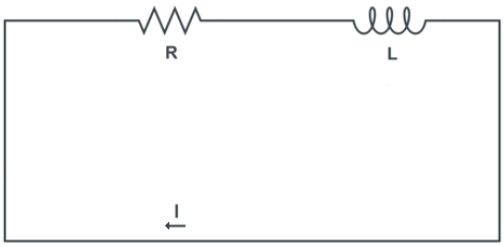

Figure 2.8: Simple protection circuit for a superconducting magnet

The integral on left in the equation 2.7 is equal to

$$\int_0^t I^2(t)\,dt = I^2 \frac{L}{2R}\left(1 - e^{-2\frac{Rt}{L}}\right) \tag{2.10}$$

If we use some typical values, as $I = 10$ kA, $L = 0.1$ H, $R = 0.05\,\Omega$, $t = 20$ ms, we obtain MIITs $\simeq 100$. If we know the material properties, and so the MIITs vs temperature function, we can find the temperature corresponding to 100 MIITs. In this way we can estimate the hot spot temperature.

2.3.2 Quench propagation velocity

Once a quench has started, the normal zone will propagate in three directions under the action of heat conduction and heat generation. In order to protect the magnet, it's important to analyze the quench propagation velocities. For details on the calculation refer to [1] .
As you can see in the fig. 2.4, if a current J_M flows in the wires, the heat generation starts when the temperature is T_g: the current divides in copper and superconductor, according to their resistance (as two resistance in parallel). In this way current in excess flows in the copper and heat is generated, and the superconductor maintain its state, but with a lower flowing current. This process continues until the temperature is T_c, and all the current flows in the copper. The power generation function is represented in fig. 2.9. We can assume that power $G = G_c$ is generated when temperature exceeds $T_s = \frac{T_g + T_c}{2}$, and there is not power generation under T_s. Under this approximation, the normal zone has a boundary with temperature T_s that travels with velocities v_L in the longitudinal direction, and v_T in the transversal direction. Under adiabatic approximations, you can prove that the longitudinal propagation velocity is

$$v_L = \frac{J}{\gamma C}\left(\frac{\rho k}{T_s - T_o}\right)^{\frac{1}{2}} \tag{2.11}$$

Regarding the transversal propagation velocity, the only differences are on the thermal conductivity and on the specific heat. It's clear that in the

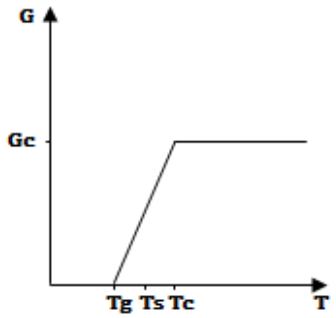

Figure 2.9: Power generation in a composite superconductor

longitudinal propagation almost only the copper is involved, otherwise in the transversal direction the superconductor and the insulation are involved, too. So, the ratio between the two propagation velocity is

$$\frac{v_T}{v_L} = \frac{C_{avm}}{C_{av}} \left(\frac{k_T}{k_L}\right)^{\frac{1}{2}} \tag{2.12}$$

where C_{avm} is the specific heat averaged only on the metallic components, C_{av} is the specific heat averaged on the whole wire cross section.

This model is strongly approximated, but it indicates the quantities involved in the quench propagation.

2.4 Quench protection

Accelerator magnets generally work at almost the highest performances that they can reach. It's so clear that a quench can always occur, and magnets are in danger without a suitable protection. There are many techniques developed in order to protect magnets, we are going to describe some of them.

2.4.1 Quench detection

The first question to answer is how to detect a quench. When a quench starts, the normal zone grows with the quench velocities indicated in the section 2.3.2. It's clear that the magnet resistance grows, too, so between the ends of the magnet a voltage $V(t) = R_q(t)I_0$ can be measured, and this voltage grows with time. So, in order to detect a quench you can measure the voltage difference between the ends of the magnet: when the voltage overcome a certain threshold a quench is detected and the protection can start.

2.4.2 External dumping resistance

The simplest way to protect a magnet is by means of an external resistance: consider the circuit in fig. 2.10. When the magnet is superconducting, the

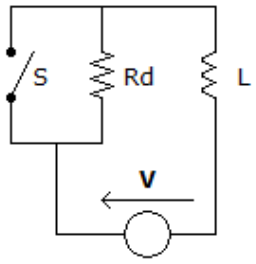

Figure 2.10: Protection system with external dumping resistance

switch is closed. When a quench is detected, the switch is immediately opened and the current starts to decay. Neglecting the normal zone resistance, a number of MIITs equal to

$$\text{MIITs} = I_0^2 t_d + \int_{t_d}^{t} I_0^2 e^{\frac{Rd}{L}(t-t_d)}\, dt \tag{2.13}$$

is developed. t_d is the time needed to reach the voltage threshold for the quench detection plus an eventual delay for the switch opening. Clearly, this time depends on the quench propagation velocities: the faster is the propagation, the faster the switch is opened, and the resultant hot spot temperature will be lower. It's so important to maintain t_d as low as possible.
The integral in the equation 2.13 depends on the dumping resistance. The current fall is faster whit a high R_d, and a minor number of MIITs is developed. So, with very high dumping resistance you should be able to carry the current to 0 in very few time, and so to maintain the hot spot temperature under a suitable level. The problem is that accelerator magnets have high inductance, so high voltage $V = L\dot{I}$ is generated between their ends. Therefore, the dumping resistance value is limited by the maximum voltage supported by the magnet. Generally, voltages over $\sim$ 1 kV can break the insulation and damage the magnet.
Protection with only dumping resistance is possible in small magnets, in some cases, because most of the energy can be extracted by the dumping resistance. This never happens in large Nb_3Sn magnets, because the stored energy to be dissipated is very high.

2.4.3 Quench heaters

We just said that in large Nb_3Sn magnets the dumping resistance cannot protect the magnet alone. Protection is so completed by means of the *quench heaters*. Quench heaters are resistive strips of steel foils in direct thermal contact with the coils, all along the magnet. When a quench is detected, heaters are immediately fired and generate heat. In this way, after a certain time t_{QH}, due to the heat diffusion in the insulation, almost all the magnet is resistive. The energy is dissipated on a larger volume, and the coil resistance R_c makes the current fall faster. The MIITs developed are

$$\text{MIITs} = I_0^2 t_d + \int_{t_d}^{t_{QH}} I_0^2 e^{\frac{Rd}{L}(t-t_d)}\, dt + \int_{t_{QH}}^{t} I_0^2 e^{\frac{Rd+R_c(t)}{L}(t-t_{QH})}\, dt \qquad (2.14)$$

In this way the hot spot temperature can be maintained under a safe level.

Chapter 3

QLASA and ROXIE validation

3.1 Quench simulation softwares

In the chapter 2 we've treated the quench analytically, and we've found some equations for the quench propagation velocities and for the hot spot temperature estimation. However, all the calculations were roughly approximated, and often they are not suitable for a detailed analysis, because the actual case is very complicated. The thermal problem discussed in the chapter 2 has to be solved considering the coupling with the electromagnetic equations: all the quantities involved in the quench propagation (as the thermal conductivity or the heat capacity) are function of the temperature, that is determined by the current decay, but the current decay too depends on the quench propagation, because it is determined by the resistance developed by the quench; moreover, the magnet resistivity is function of the temperature, and of the magnetic field too (at very low temperature, as in the accelerator magnets case, the magneto-resistance is not negligible), so resistivity depends on the current decay. In practice, in the actual case all the quantities involved are coupled each other, and an analytical treatment is impossible to be realized.
Along the years, quench simulation softwares have been developed in order to simulate the quench propagation and protection as similar as possible to the actual case. I've used two of these codes, QLASA and ROXIE, and I'm going to briefly present them. These two codes are very useful for a cross comparison, because they have a very different approach to the problem, as we are going to see.

3.1.1 QLASA

QLASA[3] is a quench simulation code written for solenoids, but it's adaptable to accelerator magnets, as we will see in the section 3.2.1.
The solenoid cross section is a whole block with the material properties averaged on the cable. The material properties are taken from the library MATPRO[6]. The approach is basically analytical. The quench starts in a zone of determinable size. The temperature of this normal zone is determined by means of the equation 2.7. Then the quench propagates, and the quench propagation velocities are calculated using the equation 2.11 and 2.12. The equation 2.12 is used for the calculation of both the axial and the radial propagation velocities: these velocities are different because of the magnetic field. It's so clear that the normal zone cross section is asymmetric, as shown in fig. 3.1. The normal zone resistance is calculated

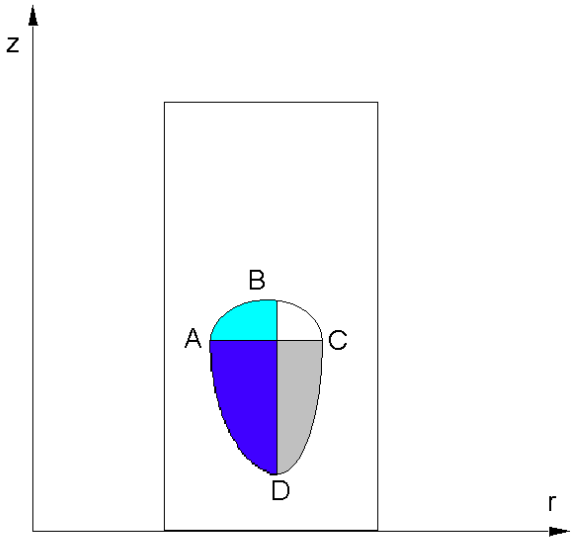

Figure 3.1: Asymmetric normal zone cross section

as

$$R = \int \rho_{vol}\left[T(\vec{x}), B(\vec{x})\right]\, dV \tag{3.1}$$

where ρ_{vol} is the resistance per volume unit, and the current is scaled according to the equation 2.9. The magnetic field is scaled linearly, according to the current. At every temporal step the normal zone is bigger, and all the calculations are repeated. The temperature of the new normal zone is set to T_g (see fig. 2.4), and then at every step it augments according to the equation 2.7, so the resistive zone has a "onion-look", where every layer has its own temperature and its own resistance. It's clear that the zone where

the quench starts has the highest temperature.
The magnetic field is set as input: it's possible to define it in the four points indicated in fig. 3.2, then the complete field map is obtained by means of

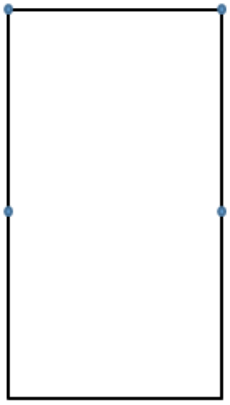

Figure 3.2: Points where the magnetic field has to be set as input in QLASA

linear interpolation and assuming top-bottom symmetry.
The strength of QLASA is surely its adaptability: the analytical approach just described can be adjusted by means of correcting factors for the quench propagation velocities. This feature is very important in order to validate the code with experimental data.

3.1.2 ROXIE

ROXIE[4] is a software originally created for the magnetic design of superconducting magnets. In the last years, a quench simulation subroutine has been implemented.
The approach is very different from QLASA. All the turns have an averaged core plus the insulation, and they are all independent each from the other. Longitudinally, it's possible to divide the turns in a maximum of 100 elements. In practice, the magnet is divided in several elements, and for each element all the properties are calculated depending on the temperature and on the field. During the quench simulation, the heat equation is solved numerically, and the temperature of each element is calculated. When the temperature of an element is high enough to quench it, the element becomes resistive and generates heat. In this way, the quench propagates in the longitudinal and transversal direction. Note that in the temperature calculation both ohmic generation and thermal conduction are involved, so there is not adiabatic approximation.

LQ cable	
Material	Nb_3Sn
Strand diameter	0.7 mm
Number of strands	27
Bare width	10.077 mm
Bare inner thickness	1.172 mm
Bare outer thickness	1.348 mm
Insulation thickness	0.125 mm
Cu/NCu	0.89

Table 3.1: LQ cable features

3.1.3 Softwares validation

All the quench simulation programs have their own approach to solve the problem, and make their own approximation. A useful manner to understand the code reliability is to compare the simulations with some experimental data. For example, the simplest comparison could be between the experimental and the simulated current decay.
QLASA and ROXIE have been used a lot for simulating $NbTi$ magnets, but they still need a validation with experimental data for the new Nb_3Sn magnets, as the MQXF will be. One of the purposes of this thesis work is to validate QLASA and ROXIE with experimental data from some Nb_3Sn magnets tested at FermiLab (Chicago-IL, USA). I'm going to present the results in the next sections.

3.2 LQ

LQ[7] (Long Quadrupole) is a two-layers Nb_3Sn quadrupole with a length of 3.7 m. The tab. 3.1 reports the cable properties. Several quench protection tests have been performed at FermiLab, and I've used some of the test data in order to validate QLASA and ROXIE.

3.2.1 QLASA geometrical transformation

We've just said that QLASA is a quench simulation program written for solenoids. It's clear that we need some adjustments in order to simulate a two-layers quadrupole. You can represent each coil of each layer with a solenoid, so the whole magnet can be described with 8 solenoids. In order to preserve the magnet resistance, it's important to preserve the coil volume in the calculation of the equivalent solenoid radius. The coil volume is equal to

$$V_{coil} = 2LNwh \tag{3.2}$$

where L is the magnet length, N the number of turns, w the cable width,

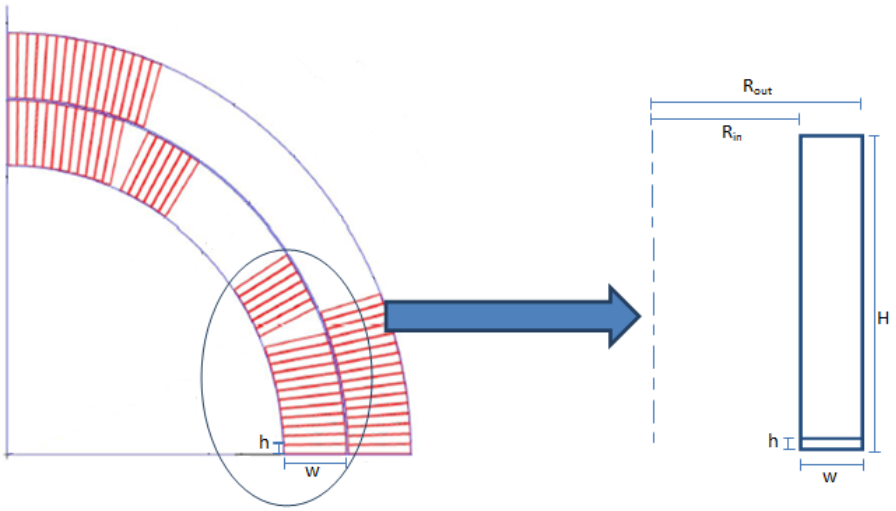

Figure 3.3: Geometrical transformation of a quadrupole coil in a solenoid

and h the cable height. We want to transform this coil in a solenoid with height $H = Nh$ and with the same volume. The volume of a solenoid is equal to

$$V_{sol} = \int_{R_{in}}^{R_{out}} H 2\pi r \, dr = H\pi \left(R_{in}^2 - R_{out}^2 \right) \tag{3.3}$$

where R_{in} and R_{out} are the inner and outer radius respectively. If we put $R_{out} = R_{in} + w$ and $V_{coil} = V_{sol}$, we obtain that the transformations

$$\begin{cases} R_{in} = \frac{L}{\pi} - \frac{w}{2} \\ R_{out} = R_{in} + w \\ H = Nh \end{cases} \tag{3.4}$$

preserve the magnet volume. This transformation can be utilized for simulating accelerator magnets in QLASA. Note that eventual spacers between the coils are not considered in this way. If you want to take them into account, you have to divide the equivalent solenoid in two solenoids with the appropriate heights.

3.2.2 QLASA magnetic field

We've just seen that the magnetic field in QLASA is an input value (see fig. 3.2). We want the magnetic field in the solenoid as similar as possible to the magnetic field in the quadrupole coil.

In a quadrupole, the peak field is on the top of the coil. If we choose to set the peak field on the top of the solenoid, too, we will have the same field on the bottom, because of the symmetry that QLASA assumes (see section 3.1.1). Generally a quench starts in the peak field zone (because there the margin to the critical current is the lowest), so in the actual case the quench propagates from the high field zone to the low field one, else in the simulation from the high field zone to the low field and then to the high field again. This difference could cause a wrong estimation of the coil resistance. So, the best choice is to set the peak field in the middle of the coil, as shown in fig 3.4. If you make this choice, you have to pay attention

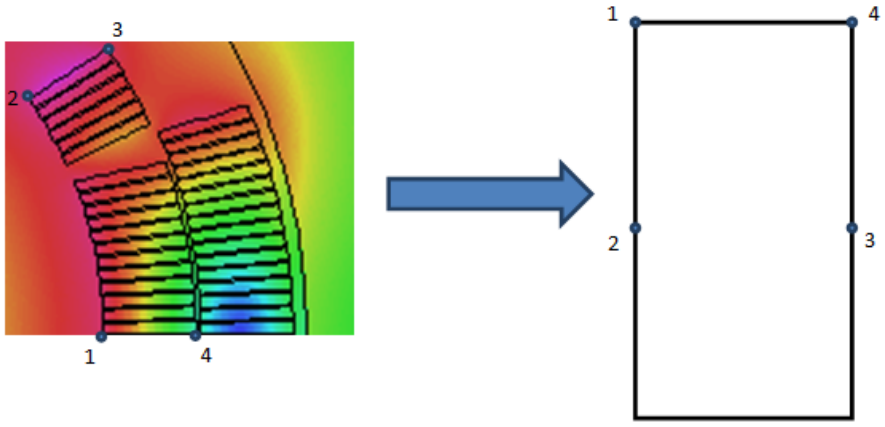

Figure 3.4: Magnetic field input in QLASA

to the quench propagation: in the actual case, the quench propagates in one direction, in the simulated case in two directions! So, in order to preserve the coil resistance, you have to divide the quench propagation transversal velocity for two, by means of the correcting factors (for details, refer to [3]).

3.2.3 Heating stations

We've just described the quench heaters in the section 2.4.3. In order to improve their performance, quench heaters generally present the *heating stations*. As you can see in the fig. 3.6, heating stations are narrower parts of the resistive strip. The heat generation is so concentrated in the heating station zone. The quench starts in several hot spots along the coil, then it propagates in the longitudinal direction. In this way, quench covers the whole magnet faster than with uniform heating stations, that spend more time in order to quench the whole windings at the same moment.
How can we simulate the heating stations with QLASA? We've just seen

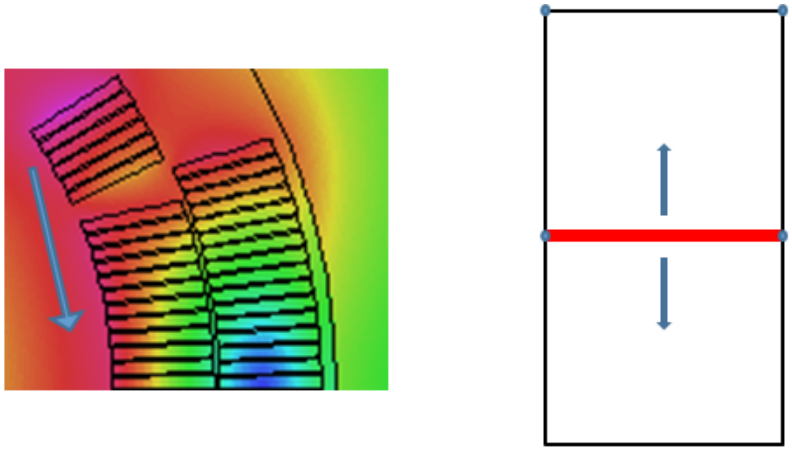

Figure 3.5: Quench propagation in the actual and in the simulated case

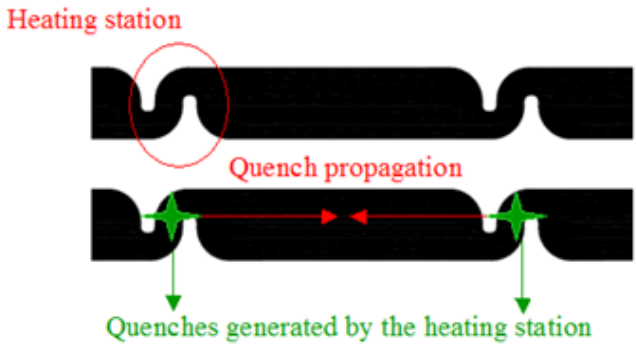

Figure 3.6: LQ-type heating stations

that quench is induced in several hot spots, but QLASA permits to start **only a quench** per solenoid. The solution is to start the quench in one point, and then make it propagate with a longitudinal velocity equal to

$$v = N_{hs} v_L \tag{3.5}$$

where N_{hs} is the number of heating stations all along the coil. This correction can be easily made by means of the quench propagation velocities correcting factors.

3.2.4 QLASA 9 solenoids model

In the section 3.2.1 we've shown that a two-layers quadrupole can be described by 8 solenoids. However, this model has a problem: QLASA permits to start only one quench per solenoid. Quench heaters are simulated as

quenches at a certain time, so in the simulation the coil where the quench starts cannot be covered by the quench heaters, else in the actual case quench heaters cover the whole magnet. I've verified that this difference cause a considerable error in the coil resistance estimation, as you can see in the fig. 3.7. This figure reports a comparison between an experimental LQ current decay

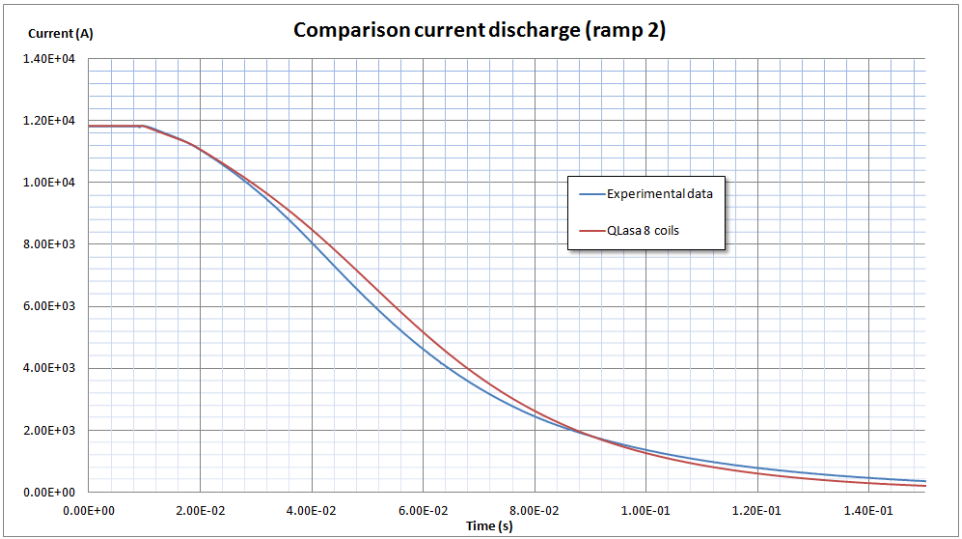

Figure 3.7: Comparison between a LQ experimental current decay and the simulated current decay by the QLASA 8 solenoids model

and a QLASA simulation with the 8 solenoids model. The initial current is 11818 A ($\sim 80\%$ of the short sample limit); the dumping resistance is 60 mΩ, and the voltage threshold 800 mV. You can see that when the heaters induce the quench (at about 20 ms), the simulated discharge is considerably slower. The time of the quench induced by heaters has been found on the experimental curve by seeking the change of slope.

In order to prevent this situation, I've developed a 9 solenoids model: the coil where the quench starts can be divided in two solenoids: If the height of the coil is H, and the quench covers a height h before the voltage threshold is reached, the solenoid where the quench starts will have a height h, the other one $H - h$. In this way, the volume is preserved, and the coil can be covered by the quench heaters. The fig. 3.8 reports the same decay of the fig. 3.7 compared with the 9 solenoids QLASA model. You can see that in this case the decay is almost perfectly coincident until 6 kA. Then, the simulated curve decays faster than the experimental one. This can be explained by the iron saturation: at very high current, the magnet inductance decreases, because the iron yoke saturates. The fig. 3.9 reports the LQ inductance calculated by ROXIE. In QLASA the inductance is an input value, and it's constant, so this effect cannot be taken into account. For the simulations, I've used the high current inductance value, so, as the

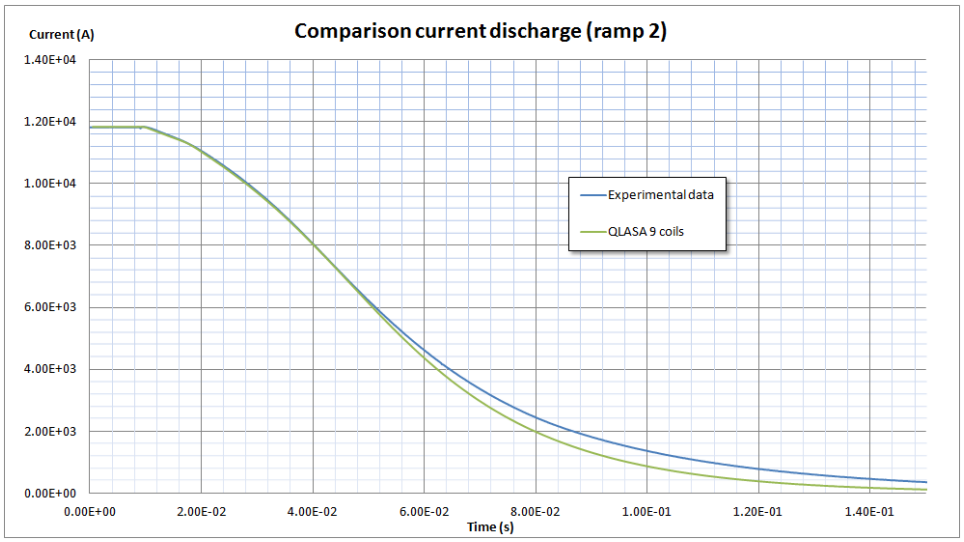

Figure 3.8: Comparison between a LQ experimental current decay and the simulated current decay by the QLASA 9 solenoids model

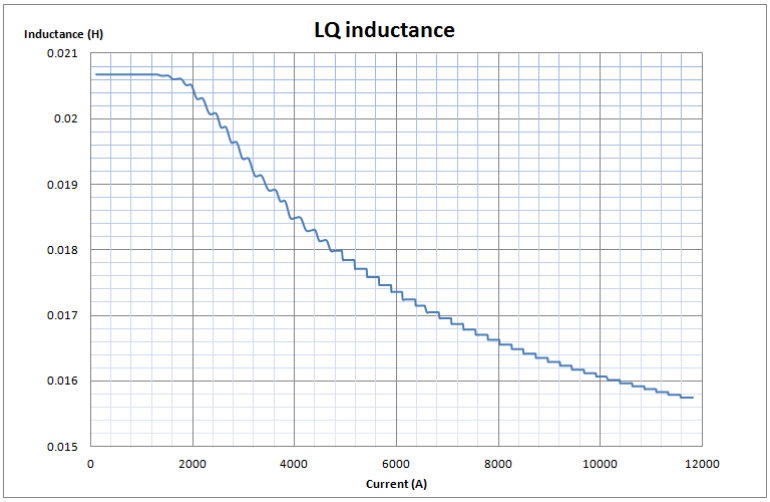

Figure 3.9: LQ inductance calculated by ROXIE

current decreases, the simulated curve is faster than the experimental one, because its inductance is not rising. This explain the difference in fig. 3.8.

Another important consideration is that the inductance value used for the simulations has been "measured" on the experimental curve: immediately after the switch opening, before the quench heaters induce quench, the inductance can be easily calculated as $L = R_d\tau$, by means of an exponential fit of the curve in order to determine τ. This calculation gives a LQ inductance value of $\sim$ 11 mH, against the value of $\sim$ 15.7 mH calculated

by ROXIE (see fig. 3.9). This indicates that the "effective" inductance is $\sim$ 30% lower than the calculated one. This could be explained as result of the high $dI/dt \simeq 60$ kA/s at the start of the decay: the energy losses due to the eddy currents in the windings and in the yoke could play a very important role, so the magnetic energy $\frac{1}{2}LI^2$ that the coils have to dissipate could be considerably lower, and this appears as a lower effective inductance. ROXIE, instead, calculates the steady-state inductance, and this effect cannot be taken into account. However, this qualitative explanation has to be confirmed, because its amount is not known.

The last important consideration is that in the simulated case and in the experimental case the switch opening is perfectly coincident. This result confirm that the model described in the section 3.2.2 describes well the quench propagation and the voltage growth.

In summary, we can conclude that the QLASA 9 solenoids model, together with the consideration made about the inductance, describes well a current discharge.

3.2.5 ROXIE model

As seen in the section 3.1.2, ROXIE doesn't need any geometrical transformation. Therefore, the magnet geometry can be perfectly described in the quench simulation, except the coil ends. The magnetic field is calculated by the program, and the iron yoke is taken into account. A first attempt is reported in fig. 3.10. The first consideration is that the switch opening

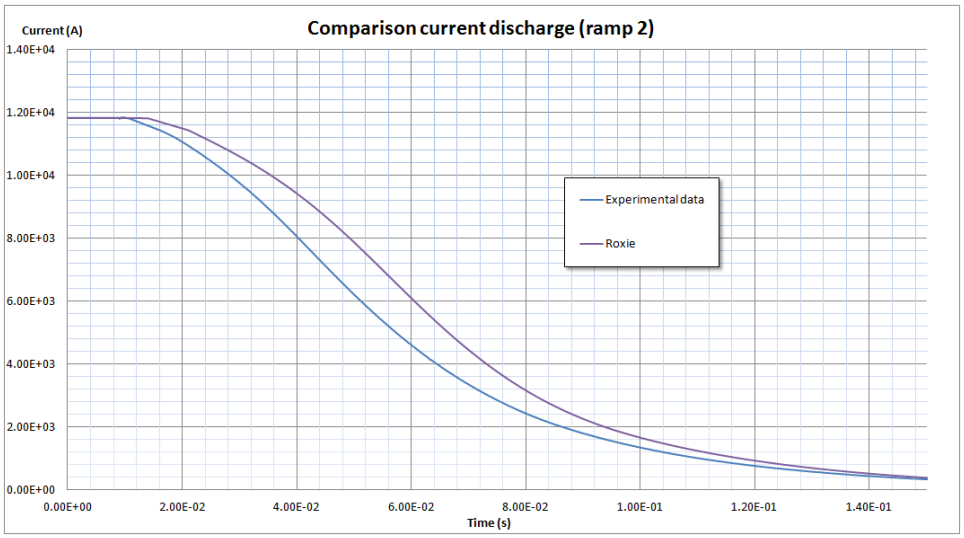

Figure 3.10: Comparison between a LQ experimental current decay and the simulated current decay by the ROXIE model

is not coincident. Therefore, the ROXIE quench propagation velocities are

underestimated, and ROXIE has a conservative behavior. It's not possible to correct directly the velocities as in QLASA, because of the different approach to solve the problem (see section 3.1.1 and 3.1.2), but you can correct the longitudinal and transversal thermal conductivity. The fig. 3.11 reports the same current discharge, with a correcting factor of 2 for both the longitudinal and the transversal thermal conductivity. You can see that,

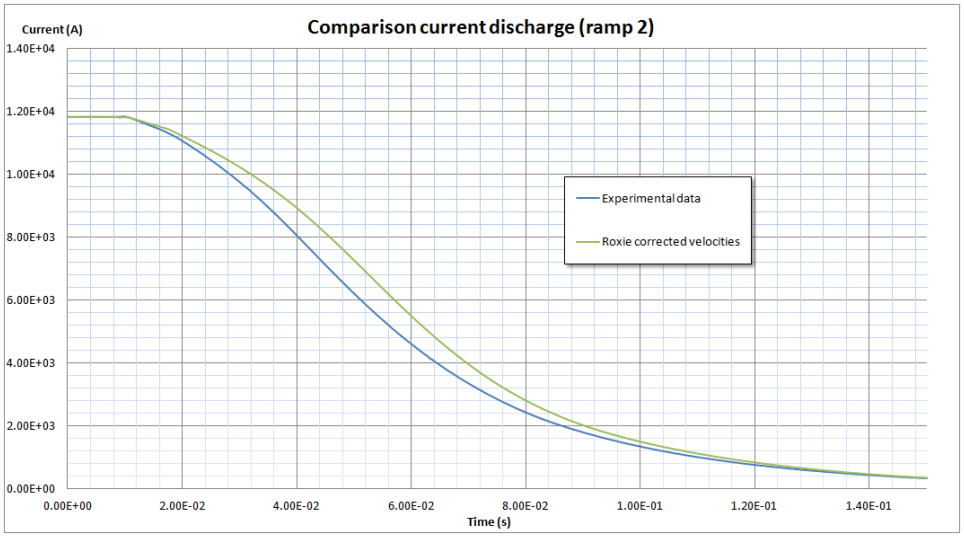

Figure 3.11: Comparison between a LQ experimental current decay and the simulated current decay by the ROXIE model with the corrected propagation velocities

thanks to the correcting factor, the switch opening is coincident, so, now, the voltage growth is simulated well. However, in both the cases when the discharge is dominated by the dumping resistance and when heaters induce the quench, the simulated current decay is slower. This is due to the fact that ROXIE calculates the steady state inductance (see fig. 3.9), so the high dI/dt effects described in the section 3.2.4 have not been taken into account. A simple way to reduce the inductance is to reduce the magnet length, but this causes a lower coil resistance when heaters induce quench. However, in the ROXIE input file it's possible to define the magnetic length without modifying the winding length, so the inductance can be reduced to the value of 11 mH at the current of 12 kA without reducing the coil resistance. Fig. 3.12 shows the same current decay considering the high dI/dt effects. You can see that now the agreement between the simulated and the experimental curve is good. In ROXIE the iron saturation is taken into account, so the final part of the decay, too, is in agreement.

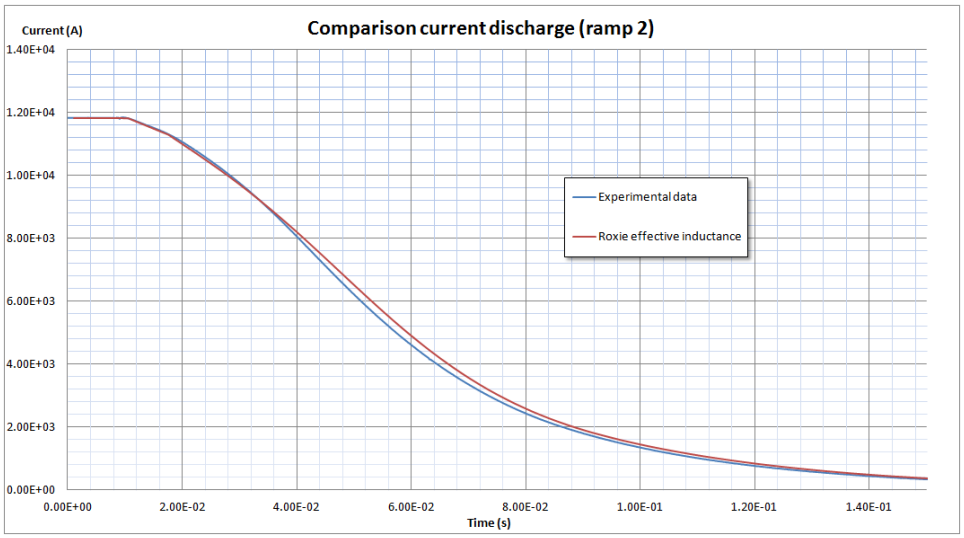

Figure 3.12: Comparison between a LQ experimental current decay and the simulated current decay by the ROXIE model with the corrected propagation velocities and considering the high dI/dt effects

3.3 HQ

The work done on LQ has to be confirmed on at least another similar magnet, in order to ensure the results. I've done some simulation on the HQ (High-field Quadrupole) test performed at Lawrence Berkley National Laboratories, (USA, California). HQ[14] is a two layer quadrupole with length of 0.8 m. The cable features are reported in the tab. 3.2.

I have to spent some words about the HQ inductance. The experimental inductance is available (see for reference [15]). I've compared this inductance with the ROXIE simulated one and with some values from exponential fit of the current decay. Results are reported in fig. 3.13. The experimental values and the ROXIE calculation agree, in fact the measures have been performed in almost steady-state. On the other hand, the effective inductance, considering the high dI/dt effects, is $\sim 30\%$ lower than the nominal one, as in the LQ case. We can conclude that the high dI/dt effects are considerable, and that they "help" the discharge, but we are not able to determine their entity.

3.3.1 QLASA simulations

I've performed simulations of a current decay with the QLASA 9 solenoids model described in the section 3.2. I've used both the nominal and the effective inductance. The results are shown in the fig. 3.14. As predictable, the measured inductance case describes well the decay, the nominal induc-

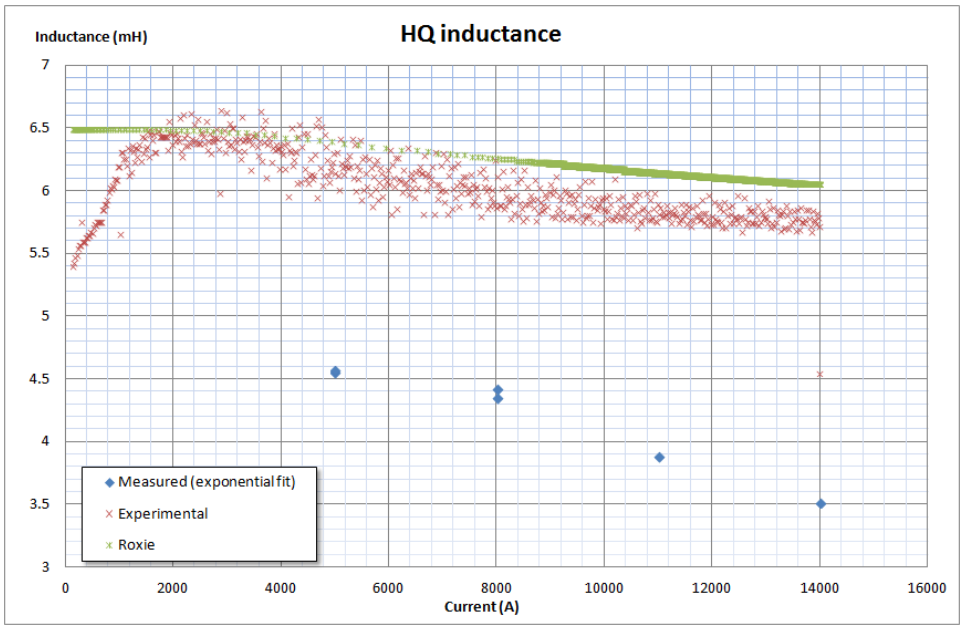

Figure 3.13: HQ inductance

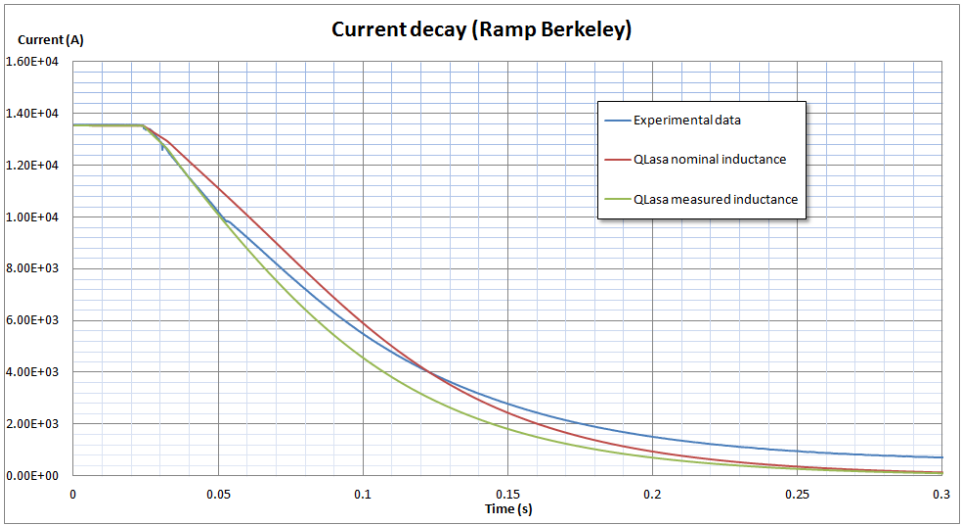

Figure 3.14: Comparison between a HQ experimental current decay and the simulated current decay by QLASA 9 solenoids model

tance one is slower. At about 50 ms, a current bump is present, due to the experimental apparatus, that presents a multi-dumping protection system. This system can not be simulated, so the simulation has to be valuated until the bump. You can easily see that the 9 solenoids model, with the effective inductance, describes well again the discharge, so the results on LQ are

HQ cable	
Material	Nb_3Sn
Strand diameter	0.8 mm
Number of strands	35
Bare width	15.15 mm
Bare inner thickness	1.332 mm
Bare outer thickness	1.535 mm
Insulation thickness	0.1 mm
Cu/NCu	0.87

Table 3.2: HQ cable features

confirmed.

3.3.2 ROXIE simulations

The same current decay in fig 3.14 has been simulated by means of ROXIE, with all the assumptions about propagation velocities made in the section 3.2.5, and with both the nominal and the measured inductance. Results are reported in the fig. 3.15. Again, all the results on LQ are confirmed.

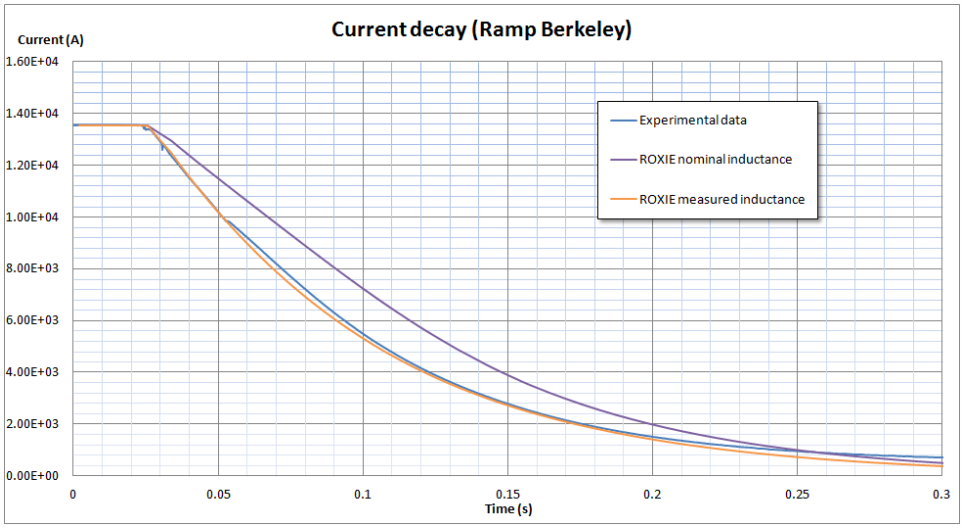

Figure 3.15: Comparison between a HQ experimental current decay and the simulated current decay by ROXIE model with the corrected quench propagation velocities

3.4 Conclusions

Both ROXIE and QLASA simulate well the current decay of LQ and HQ with the assumptions made in this chapter. The great agreement on LQ is confirmed by the fig. 3.16, that reports the MIITs developed during the three current discharges that I have simulated for the validation work. The

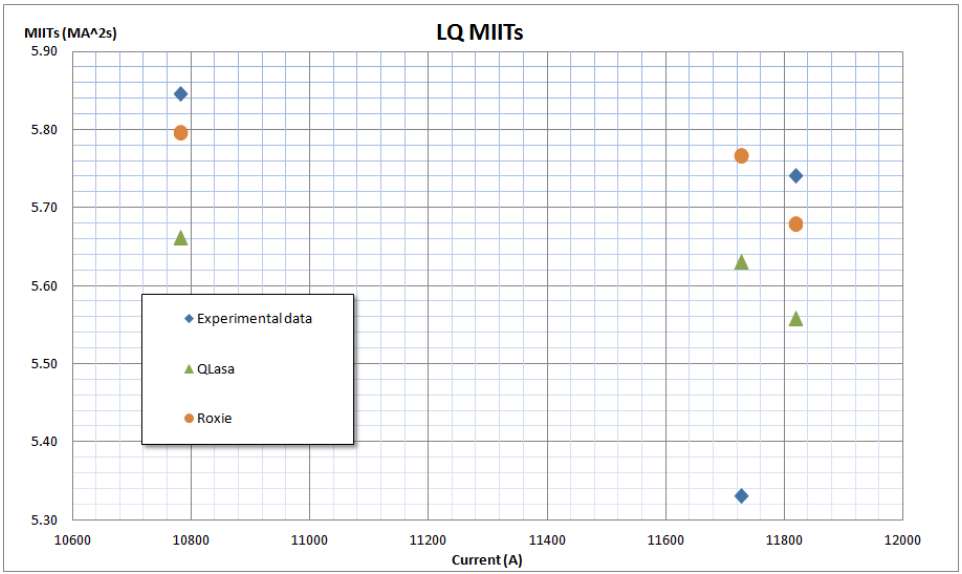

Figure 3.16: LQ MIITs from experimental data, QLASA 9 solenoids model and ROXIE model with corrected quench propagation velocities

point at $\sim$ 11700 A is a multiquench (the quench start in more than one point, so the voltage growth is faster, the voltage threshold is reached in less time and less MIITs are developed), so it cannot be compared with simulations. However, you can see that QLASA differs of about the 3% from the experimental data, ROXIE of about 1%. The great agreement, however, is accompanied by two questions:

- the inductance has been "measured" by exponential fit in both HQ and LQ, and in both the case it was $\sim$ 30% lower than the nominal one. However, the reason of this difference is not well known (it could be due to eddy currents, but a calculation is needed in order to establish their entity), so it's impossible to predict the effective inductance for a magnet in the design stage. However, we commit a conservative error using the nominal one;

- the heaters delay time has been "measured" on the current decay, seeking the change of slope. But we don't know what's the right delay time for a magnet in design stage. A parametric study for the MQXF

will be available, considering some simulations made in order to predict heaters delay time (see for reference [10]).

In conclusion, ROXIE and QLASA have been validated for Nb_3Sn magnets, so they have been used for simulating the MQXF magnet designed for the LHC luminosity upgrade, considering all the assumptions made in this chapter. The results are reported in the section 4.3.

Chapter 4

MQXF analysis

4.1 MQXF

In the 2020 LHC luminosity will be upgraded. Superconducting quadrupoles in the inner triplet of the low β insertions will play a very important role, because they are responsible of reducing the beam transversal size. Particle interactions rate can be increased by means of strong focusing superconducting quadrupoles, and MQXF is being designed in order to do that.
MQXF is a new generation superconducting two layers-quadrupole with a length of 8 m, an aperture of 150 mm, and windings made in Nb_3Sn. Tab. 4.1 shows the cable features. The tab. 4.2 shows the MQXF operational values. Fig. 4.1 shows the magnetic field plot and the MQXF cross section.

MQXF is designed for working at very high performances, so its protection study is very important, in order to don't damage the magnet. This chapter presents all the work done for predicting the MQXF hot spot temperature when a quench occurs.

MQXF cable	
Material	Nb_3Sn
Strand diameter	0.85 mm
Number of strands	40
Bare width	18.638 mm
Bare inner thickness	1.462 mm
Bare outer thickness	1.673 mm
Insulation thickness	0.15 mm
Cu/NCu	1.13

Table 4.1: MQXF cable features

MQXF operational values	
Current	17300 A
Gradient	140 T/m
Peak field	12.2 T
Temperature	1.9 K
Inductance	8.27 mH/m

Table 4.2: MQXF operational values

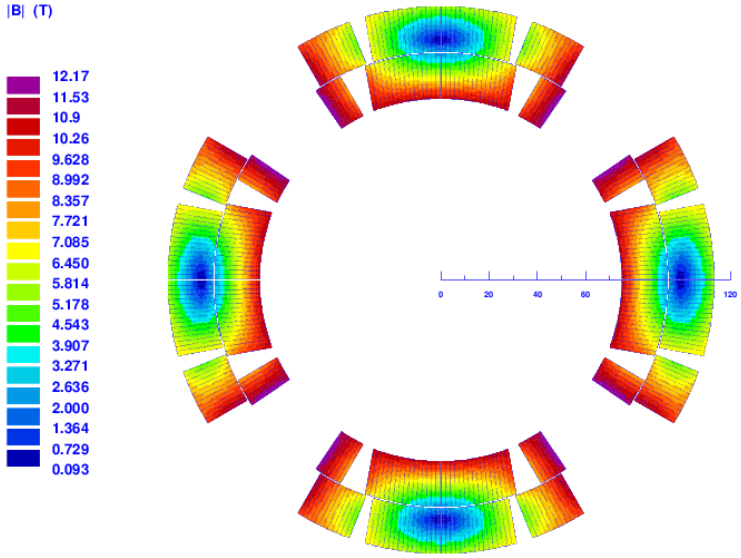

Figure 4.1: Magnetic field on the MQXF cross section

4.1.1 MIITs calculation

First of all, it's important to verify that the MIITs calculated by the simulation codes are similar, in order to be sure that results about hot spot temperature are comparable. The fig. 4.2 shows the MIITs calculated from the time integration of current decay simulated by QLASA and ROXIE, and from the direct integration of the material properties at a representative magnetic field of 12 T (see the equation 2.7). As expected, the agreement is excellent, because the two codes use the same material properties (from the library MATPRO[6]).
The limit value for the hot spot temperature has been set to 350 K. You can see in fig. 4.2 that a number of MIITs minor than 35 has to be developed, in order to preserve the magnet safety.

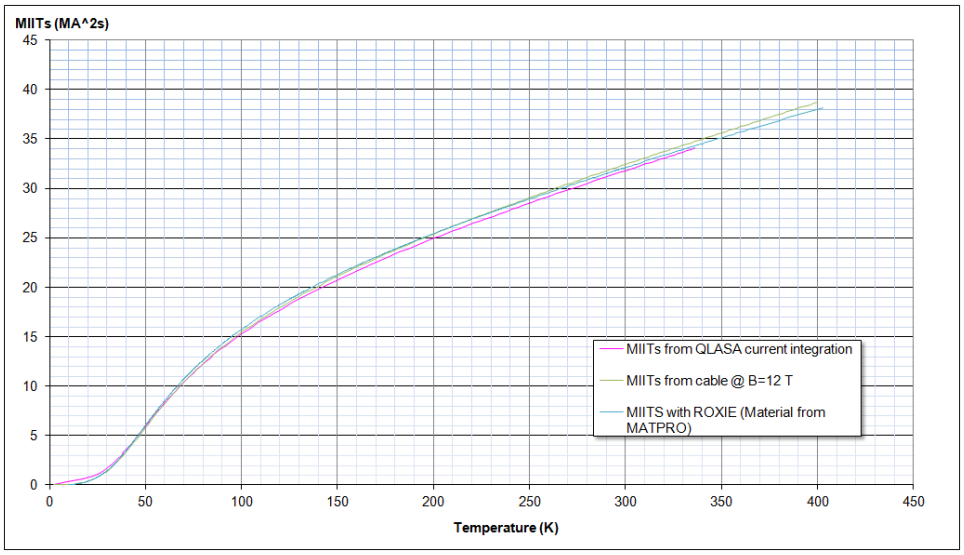

Figure 4.2: MQXF MIITs from ROXIE, QLASA and material properties at 12 T

This calculation ensures that results from QLASA and ROXIE are comparable.

4.2 Hot spot temperature estimation before codes validation

As shown in the chapter 3, QLASA and ROXIE have been validated with experimental data from LQ and HQ. Before doing that, a preliminary work had been done for the hot spot temperature estimation. In this work, the quench propagation velocities have been taken from ROXIE and corrected in QLASA by means of the quench propagation velocity correcting factors.

4.2.1 Resistive voltage growth

The fig. 4.3 represents the resistive voltage growth simulated by QLASA and ROXIE. You can see that, without correcting the propagation velocities, the propagation simulated by QLASA is very faster. Differences are due to the very different approach of the two codes (remember that QLASA uses analytical formulas for the quench propagation velocities, ROXIE solves the heat equation). You can note, too, that ROXIE is sensible to the longitudinal discretization. A thin discretization is better, in order to avoid too high steps (as in the blue curve): long elements have a high resistance, so, when they quench, the voltage step is high and the time needed to reach the voltage threshold could be distorted.
Data from QLASA with corrected propagation velocities and from ROXIE

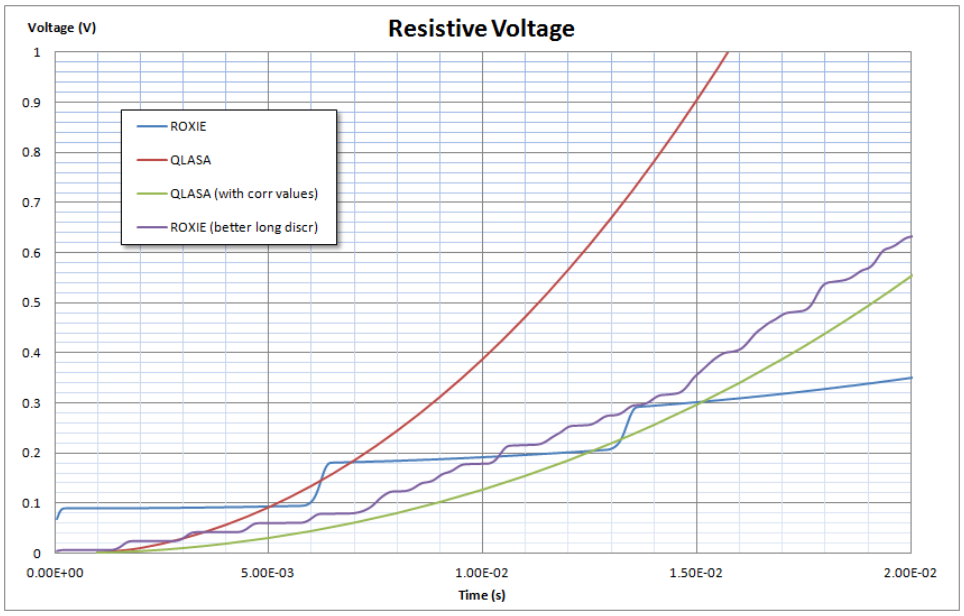

Figure 4.3: Voltage growth simulation by QLASA and ROXIE

with a thin longitudinal discretization are similar, and they have been used in the simulations for the time needed to reach the voltage threshold.

4.2.2 Hot spot temperature estimation assuming outer and inner quench heaters

As preliminary work, a study of the hot spot temperature has been carried on assuming a very optimistic behavior of the quench heaters. In the simulations shown in this section the protection heaters induce quench in both the layers at the same time. In reality, only the external layer will be covered by the protection heaters, because of the very small gap between the two layers, where it's impossible to set a quench heater. The fig. 4.4 shows a parametric study of the hot spot temperature with the assumption just described. The delay time indicated in the x-axis is the time between the voltage threshold reaching and the effective start of the quench induced by heaters. Heaters are supposed to induce the quench on the whole magnet at the same time. The dumping resistance chosen for these simulations is $Rd = 0.058$ mΩ, and the correspondent voltage between the coil ends is 1 kV.
These results are not very considerable for the hot spot temperature estimation, because of the rough approximations on the quench heaters, but an interesting result is that ROXIE estimations are about 10 K lower than QLASA ones. In fig. 4.5 you can see that the temperature difference is developed mostly at the end of the simulation. This difference is so probably

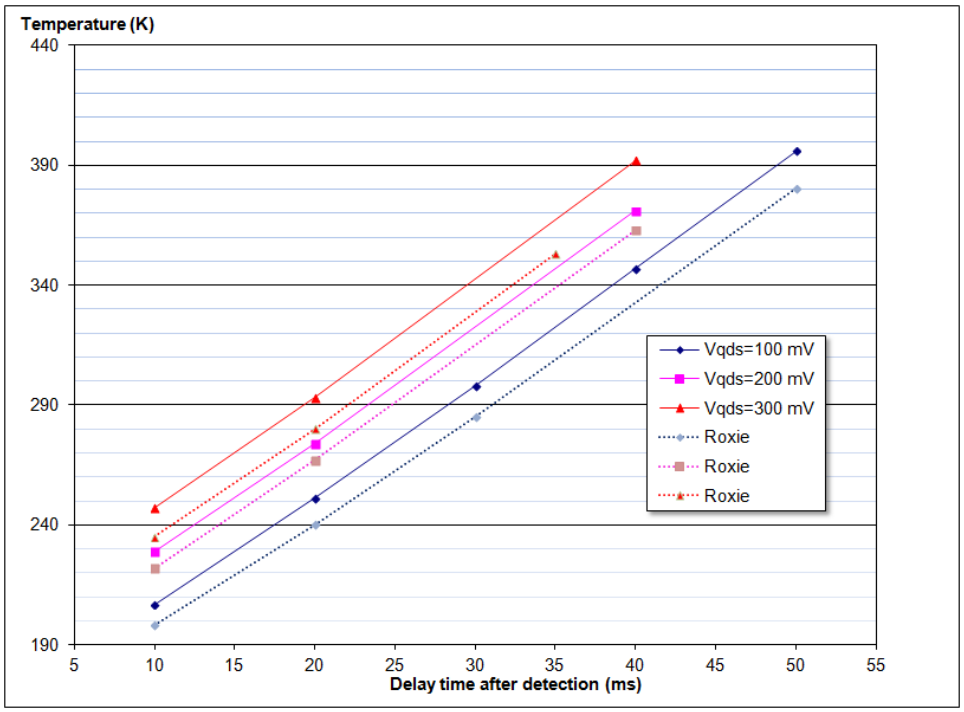

Figure 4.4: MQXF hot spot temperature assuming quench heaters on both the layers

due to the fact that QLASA does an adiabatic approximation for the hot spot temperature calculation, whereas ROXIE considers the thermal conductivity too, so at the end of the simulation the temperature rise is slower.

4.2.3 Hot spot temperature estimation assuming only outer quench heaters

MQXF will be provided by quench heaters only for the external layer. A more realistic study has been done with ROXIE: heaters induce quench only on the outer layer, then the quench propagates in the inner layer that is in thermal contact with the outer one. The heat diffusion time between the two layers has been calculated by ROXIE, and it is of about 100 ms. The fig 4.6 shows the results of this study. The fig. 4.7 reports a comparison between the study shown in the fig. 4.6 and the ROXIE study shown in the fig. 4.4, in the case of dumping resistance equal to $R_d = 0.058\,\Omega$. You can see in the fig. 4.7 that the difference between the two cases is of about 60 K. This confirm that the approximation made in the section 4.2.2 was very rough. This result shows that the magnet resistance dominates the dumping resistance, as you can see in the fig. 4.8. There are not significantly differences in varying the value of the dumping resistance, whereas the decay

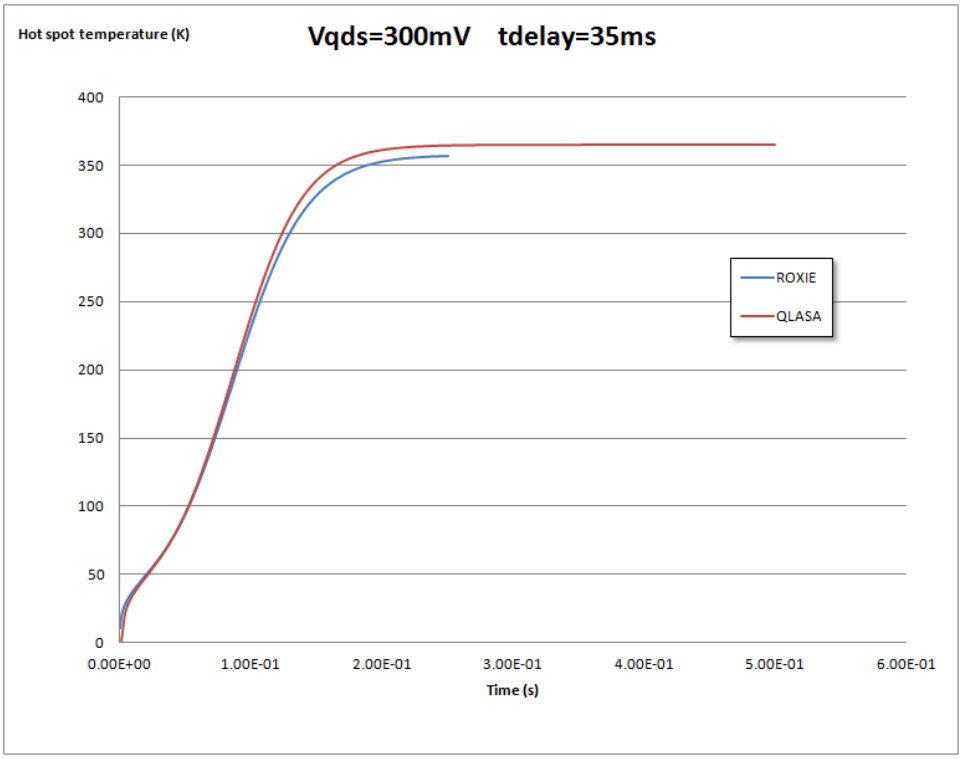

Figure 4.5: MQXF hot spot temperature vs time simulation for one of the cases reported in fig. 4.4

with only outer quench heaters is considerably longer.
The same study can be made with QLASA, using the value calculated by ROXIE for the heat diffusion time between the two layers. Results are reported in the fig. 4.9. A comparison between the results of QLASA and ROXIE considering only the external heaters is reported in the fig 4.10, in the case of $R_d = 0.058\,\Omega$. The comparison between the two codes confirms the considerations just made in the section 4.2.2.

4.2.4 Conclusions

The hot spot temperature estimations from these preliminary simulations are not reliable, because they still need a validation with experimental data. However, we can already conclude that

- QLASA and ROXIE have a very similar behavior, if the quench propagation velocities calculated by QLASA are adequately corrected. This result is not obvious, because of the very different approach of the two codes in solving the quench propagation problem.
- We have few time for detecting the quench and active the whole pro-

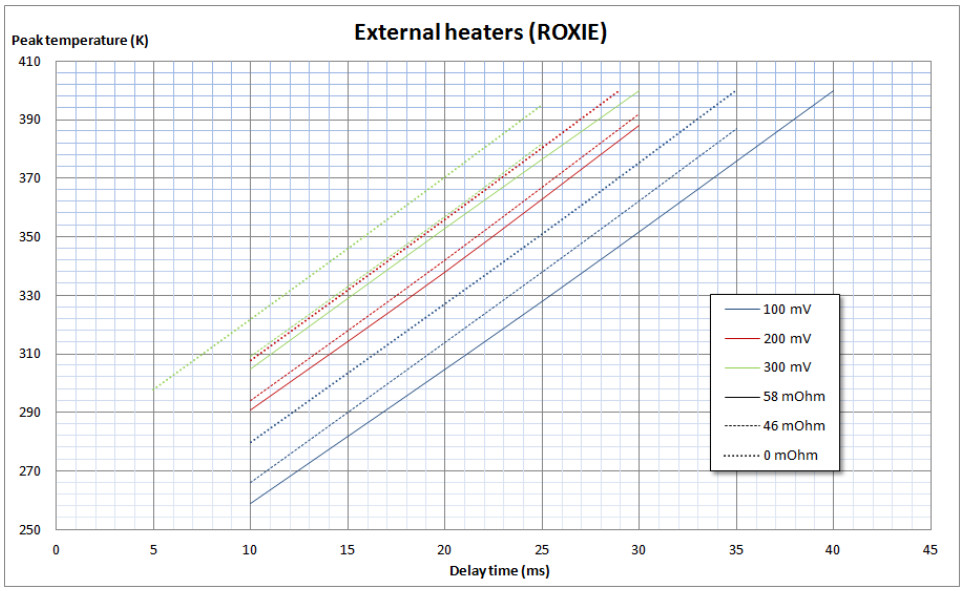

Figure 4.6: MQXF hot spot temperature by ROXIE, considering quench heaters only on the external layer

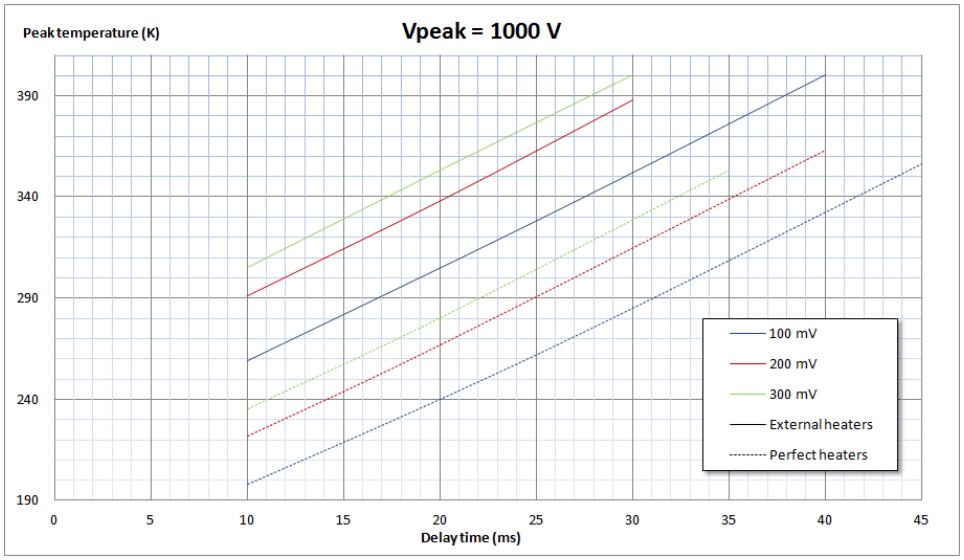

Figure 4.7: MQXF hot spot temperature calculated by ROXIE. Comparison between the cases of only outer QH and both outer and inner QH

tection system.

This last result is shown in the fig. 4.11. This graph shows the MIITs produced only during the current decay from the switch opening. This MIITs estimation is quite reliable, because it doesn't depend on the initial

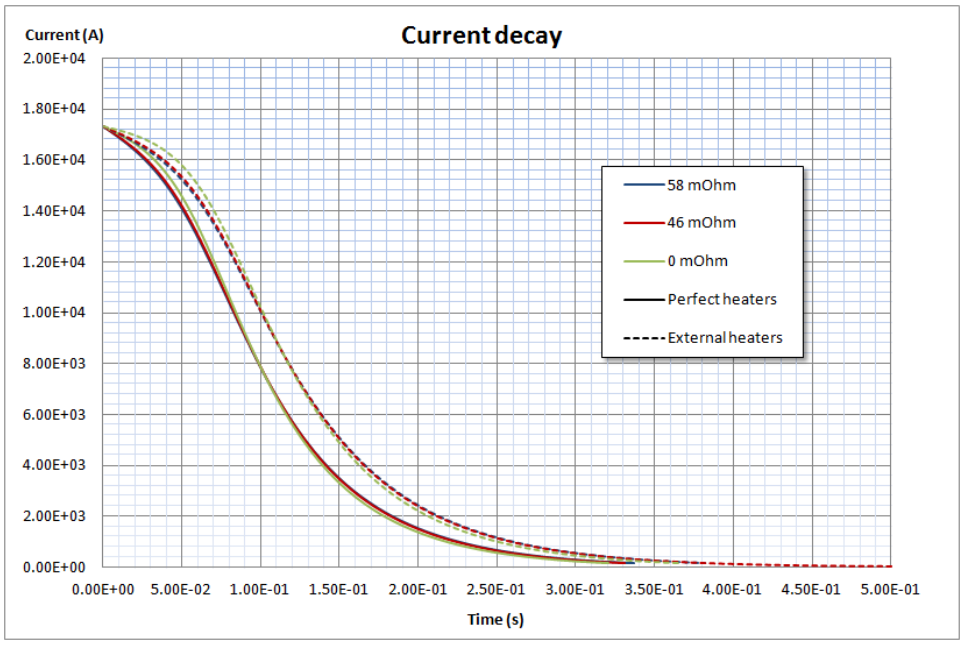

Figure 4.8: Current decay simulated by ROXIE. Comparison between the cases of only outer QH and both outer and inner QH

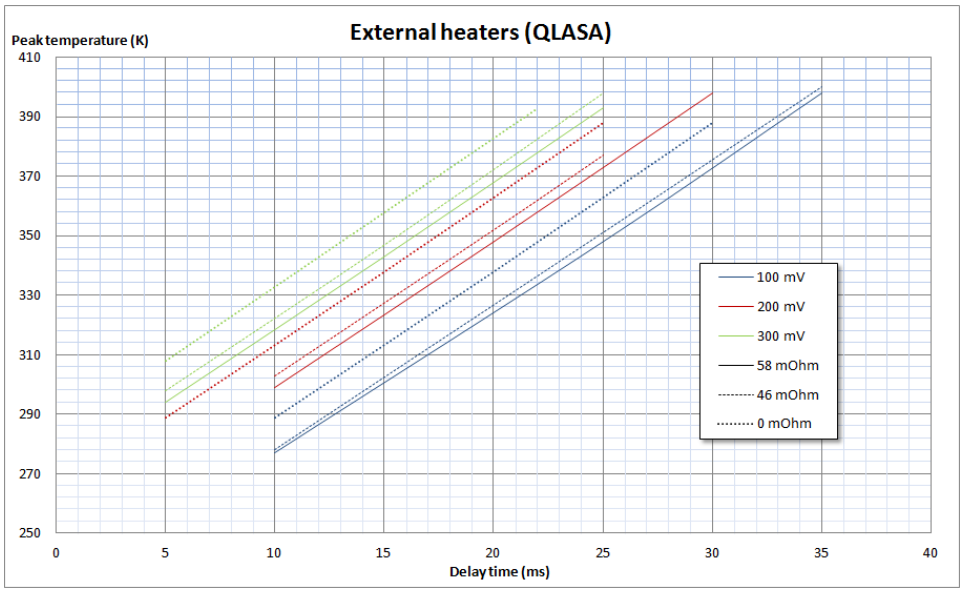

Figure 4.9: MQXF hot spot temperature by QLASA, considering quench heaters only on the external layer

quench propagation, that is the part that has to be validated. MIITs developed starting from the switch opening are almost independent on our acts

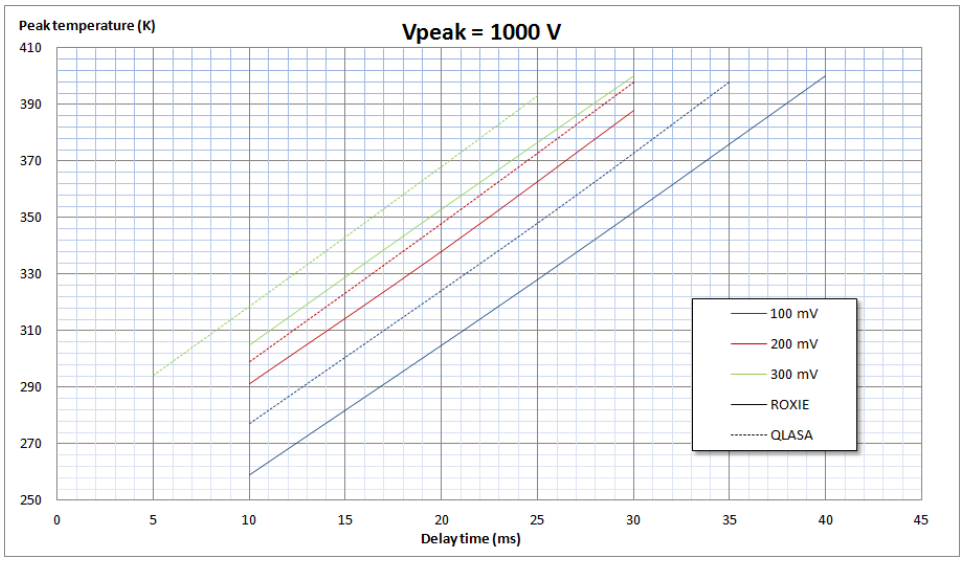

Figure 4.10: MQXF hot spot temperature comparison between QLASA and ROXIE, considering QH only on the outer layer

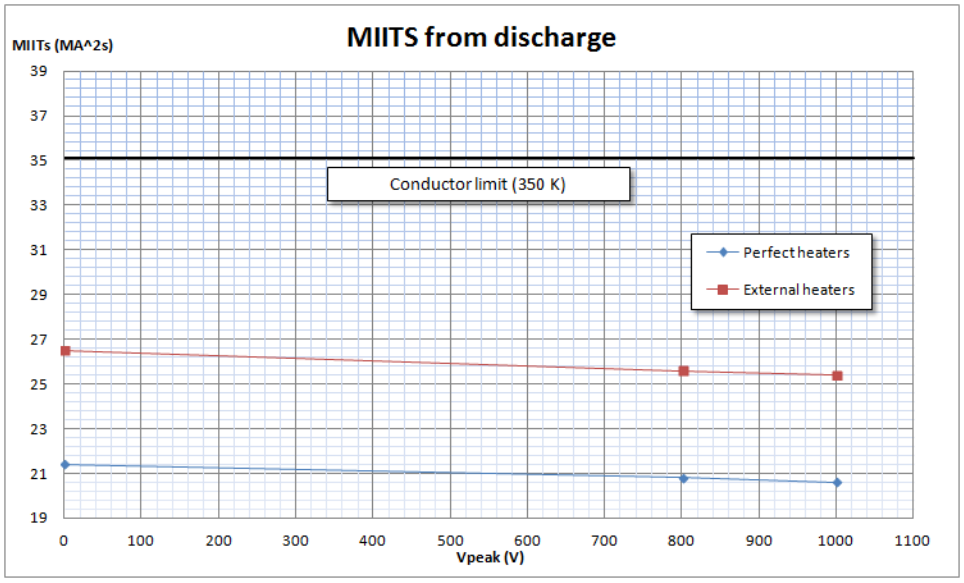

Figure 4.11: MIITs produced by the only current discharge, starting from the switch opening. The dumping resistance considered is $R_d = 0.058\,\Omega$

(heaters delay time depends on the heat diffusion time in the insulation, and dumping resistance is limited by the maximum voltage between the coil ends), so in the fig. 4.11 we can find the maximum number of MIITs that can be developed from the start of the quench to the switch opening. You can see that we have only $\sim$ 9 MIITs to the conductor limit of 350 K, so

we have $\sim$ 30 ms to detect the quench, open the switch and fire the quench heaters. The simulation of this part of the quench protection strongly depends on the quench propagation velocities, so a validation of the codes with experimental data is very important.

4.3 Hot spot temperature estimation after codes validation

In the chapter 3 we have seen that ROXIE and QLASA have been validated with some experimental data, and we have seen in details the assumptions made in the validation work. All the assumptions are repeated in the study reported in this section.

4.3.1 New quench heaters design

A new quench heaters design is under development for the MQXF protection. The fig. 4.12 shows a scheme. You can see that the heating stations are

Figure 4.12: Quench heaters design for the MQXF

composed by three narrow strips with different length. There are two quench heaters of this kind, one designed for the high field block, one for the low field block. The width of the three narrow strips is different in the two zones, and the strips length is optimized for quench as faster as possible the turns under them. The aim of this design is to quench as fast as possible the whole coil. Simulations[10] show that such quench heaters induce the quench 17 ms after the firing in the high field zone, 25 ms after the firing in the low field zone (these are average times for the whole zones); then, the quench propagates in the longitudinal direction and covers all the turns 26 ms after the firing in the high field zone, 37 ms after the firing in the low field zone. These numbers will be used in the ROXIE and QLASA simulations.
Quench heaters cover only the external layer, then the quench propagates to the inner layer for thermal conduction. Some experimental data (G. Chlachidze, colloquial) show that the outer-inner layer quench propagation takes less than 20 ms at the 80% of the short sample limit current (as in the MQXF case). We will assume that the quench takes 20 ms to propagate from the outer to the inner layer.
QLASA permits to calculate the heat diffusion time between the two layers, and the result is 30 ms. However, the experimental data are more reliable,

because QLASA uses analytical formulas, and it doesn't take into account the insulation between the layers, but only the cable insulation.

4.3.2 Time-line and protection parameters

The fig. 4.13 reports the time-line of the events.
The voltage threshold for the quench detection is a key-parameter: it's im-

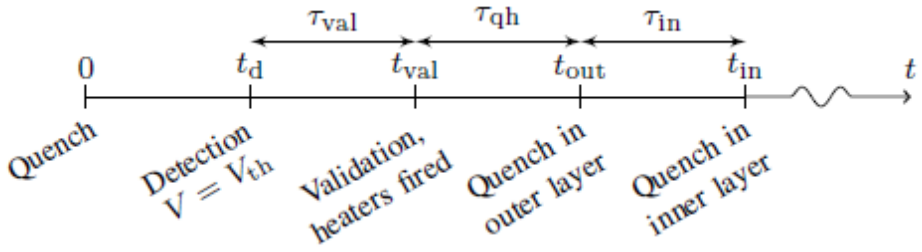

Figure 4.13: Time-line of the events in the quench protection

portant to choose it as low as possible, in order to reduce the operation time; on the other hand, a too much low threshold could cause false quench detections, because of the electronic noise or of some transient instabilities of the superconductors. For these reasons, the two limit values of 100 and 200 mV have been examined for the hot spot temperature estimation.
The thresholds chosen are low enough to need a *validation* time (τ_{val} in the fig. 4.13). If during this time the voltage rests over the threshold, the quench protection system is activated (the switch is opened and the quench heaters are fired). A validation time of 10 ms has been chosen.
The switch opening is not simultaneous to the validation, but 1 ms is needed.
The heaters delay time (τ_{qh}) is the time that elapses from the firing to the effective start of the induced quench. Some values are reported in the section 4.3.1, but also an optimistic case of 10 ms to start a quench in the high field zone has been considered for a complete parametric study.
Quench heaters cover only the external layer. As just said in the section 4.3.1, the outer to inner layer quench propagation time chosen is 20 ms. In order to be conservative, the quench is assumed to propagate in the inner layer only in the high field turns, then only the transversal propagation is considered.

4.3.3 Hot spot temperature estimation with QLASA

Three cases have been taken into account for doing the simulations:

- every magnet (8m) is provided of a dumping resistance of 46 mΩ (at which correspond a maximum voltage of 800 V between the coil ends)

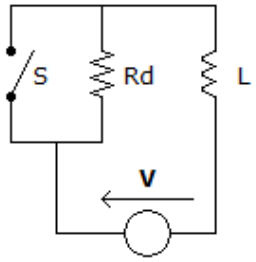

Figure 4.14: Protection scheme: every magnet is protected by its own dumping resistance

or of 58 mΩ (at which correspond a maximum voltage of 1000 V between the coil ends);

- the same dumping resistance protects a string of two magnets (simulated as one magnet of double length 16m);
- there is not dumping resistance; in this case, the discharge depends on the ratio $L/R(t)$, so it's independent on the magnet length (both the inductance and the coil resistance double, if the length doubles).

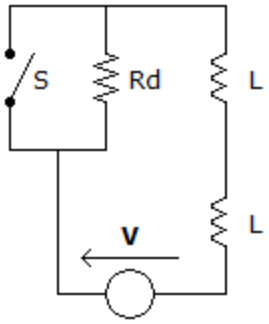

Figure 4.15: Protection scheme: a string of two magnets is protected by a dumping resistance

The fig. 4.16 and 4.17 report the hot spot temperature calculated in function of the heaters delay time. The x-axis indicates as reference the delay time from the heaters firing to the quench induced by the heating stations in the high field zone (see section 4.3.1). Together with the 17 ms discussed in the section 4.3.1, a more optimistic 10 ms case has been considered. The red horizontal line indicates the limit of 350 K. You can see that the cases without dumping resistance (blue curves) are almost equivalent, as expected; instead, in the cases of 46 (orange curves) and 58 (green curves) mΩ the 16m case show a temperature increase of $\sim$ 10 K. This is due to the fact

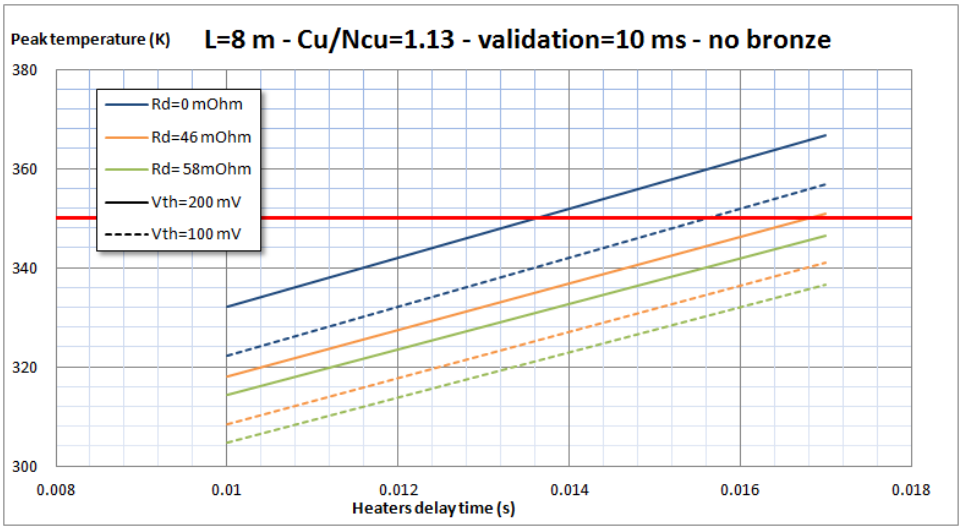

Figure 4.16: MQXF hot spot temperature estimation with QLASA for the protection scheme indicated in fig. 4.14

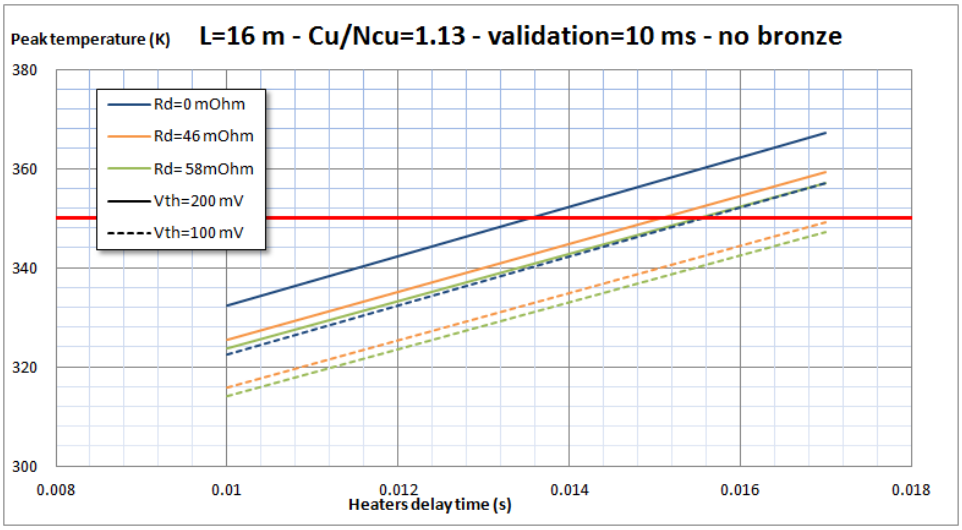

Figure 4.17: MQXF hot spot temperature estimation with QLASA for the protection scheme indicated in fig. 4.15

that when the switch is opened the constant time L/R_d is bigger, so the current decrease is slower. The two voltage thresholds considered ($200mV$ for the continue lines, 100 mV for the dashed lines) show a difference of again $\sim$ 10 K.
The same study has been repeated for a higher Cu/NCu (Copper-NonCopper ratio) value, that has been set to 1.2, against the nominal value 1.13 (see tab. 4.1). The considerations are the same of the case with the nominal

Cu/NCu, but a slight overall temperature decrease of about $\sim 2.5\%$ occurs. This is due to the higher copper quantity in the cable: copper has a heat capacity higher than niobium-tin, and a lower resistivity, so, at equality of energy to be dissipated, the temperature rise is less (see eq. 2.8).

All the study has been repeated considering a certain amount of bronze

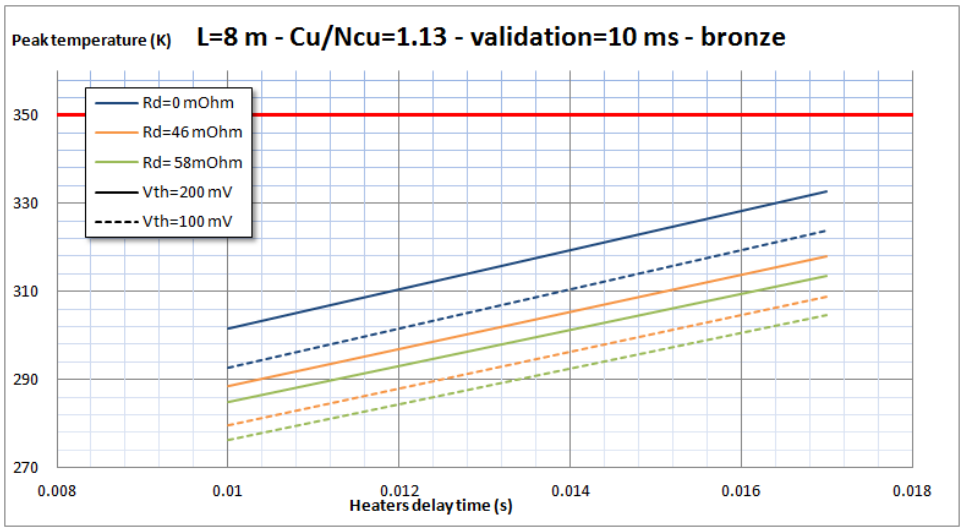

Figure 4.18: MQXF hot spot temperature estimation with QLASA for the protection scheme indicated in fig. 4.14, with a fraction of residual bronze

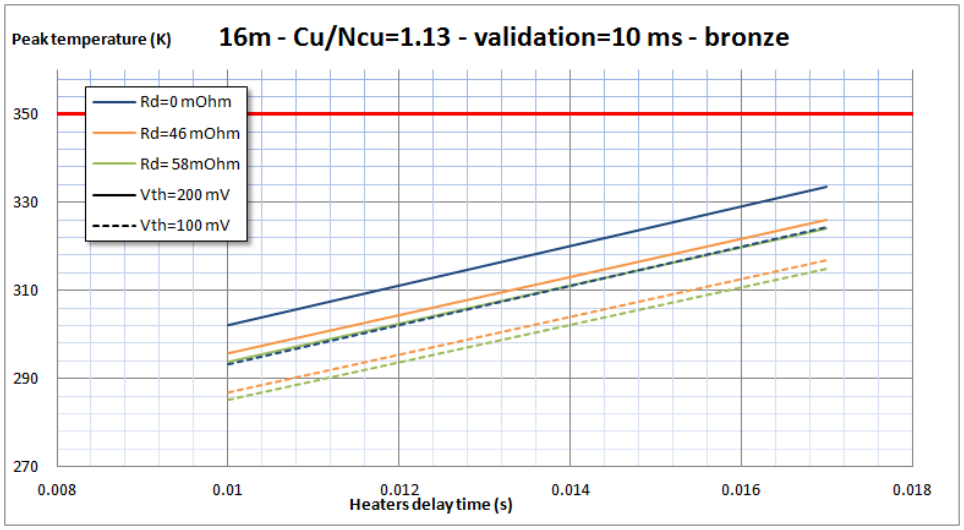

Figure 4.19: MQXF hot spot temperature estimation with QLASA for the protection scheme indicated in fig. 4.15, with a fraction of residual bronze

in the cable: the realization of Nb_3Sn windings is very complicated, mainly

Copper	0.342
Niobium-Tin	0.301
G10	0.356

Table 4.3: MQXF cable material fractions without considering bronze (Cu/NCu=1.13)

Copper	0.342
Niobium-Tin	0.202
G10	0.356
Bronze	0.1

Table 4.4: MQXF cable material fractions considering bronze (Cu/NCu=1.13)

because of the superconducting filaments brittleness. Therefore, cables composed by bronze and niobium are wound in coils, then the coils are treated with heat, and in this stage the tin is delivered by the bronze and binds to the niobium, forming the Nb_3Sn. Some analysis (A. Ghosh, private communication) show that about 1/3 of the bronze doesn't react, so this number has been used in the simulations. The tables 4.3 and 4.4 reports the material fractions in the cable for the two cases considered. The fig. 4.18 and 4.19 report the results. All the considerations made until now are the same, but the hot spot temperature estimation is lower of $\sim 10\%$. The explanation is similar to the case of the higher Cu/NCu, because the bronze has a heat capacity higher and a resistivity lower than the niobium-tin.

4.3.4 Hot spot temperature estimation with ROXIE

The same study presented in section 4.3.3 has been performed again using ROXIE. The approach to the problem is quite different, because ROXIE cannot simulate heating stations, but the quench induced by heaters has to start at the same time in the whole interested turns. The possible choices are the time when quench starts under the heating stations (17 ms, see section 4.3.1), or the time when the quench is propagated in the whole turn (26 ms, see section 4.3.1). However, I've verified with QLASA that the design described in the section 4.3.1 is very efficient, and no substantial differences occur in the QLASA simulations considering the quench induced by the heating stations or induced in the whole turns at the same time. Probably, this is due to the fact that, in the time of the longitudinal propagation, the integral of the current in the two cases is not so different, because the discharge is still dominated by the dumping resistance, so the MIITs developed are almost the same. Therefore, the time of the quench induced by the heaters in ROXIE is the same considered in QLASA.

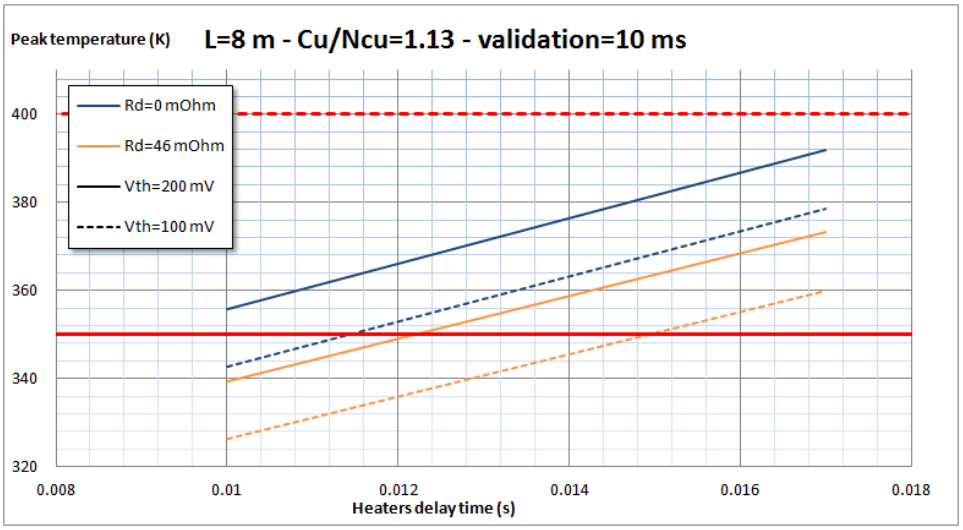

Figure 4.20: MQXF hot spot temperature estimation with ROXIE for the protection scheme indicated in fig. 4.14

As in QLASA, the propagation in the inner layer is considered with a delay of 20 ms, and it occurs only in the high field turns, then the quench propagates only in the transversal direction.
Only the nominal dumping resistance of 46 mΩ has been considered, because, as seen in the section 4.3.3, the case of 58 mΩ is very similar, and the ROXIE simulations need much more computing time than the QLASA ones. The fig. 4.20 and 4.21 report the results. The red dashed line indicates

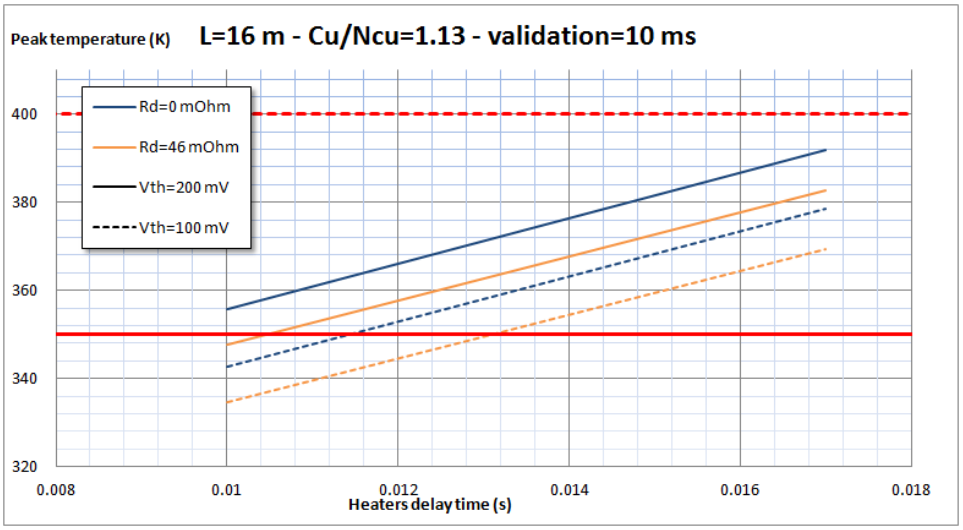

Figure 4.21: MQXF hot spot temperature estimation with QLASA for the protection scheme indicated in fig. 4.15

the highest value of temperature that a magnet can reach; over this value, the epoxy resin melts, and dangerous damages can occur.
Also in this case a study with a higher value of Cu/Ncu=1.2 has been considered, and again a hot spot temperature decrease of about 2.5% is verified. The study with the residual bronze is impossible with ROXIE, because in the cable definition you can only set the Cu/NCu, and all the NCu is superconductor.

4.3.5 Comparison between ROXIE and QLASA results

Comparing the fig. 4.16 to 4.20 and 4.17 to 4.21, you can see that ROXIE gives a more conservative estimation of the hot spot temperature. This is mainly due to:

- the voltage growth in ROXIE is slower (no correcting factors have been considered) of about 1.5 ms, so the switch is opened later in the ROXIE simulations;
- the transversal propagation in the inner layer in ROXIE is much slower: in QLASA the whole inner layer is quenched in about $60 - 70$ ms, else in ROXIE the propagation doesn't cover the whole layer! This causes a difference in the coil resistance estimation.

ROXIE simulations have been repeated considering that at t_{in} (see fig 4.13) the quench propagates in the whole inner layer. This approximation is less conservative than the QLASA one, in fact in this case the hot spot temperature estimation is about 2.5% lower than in the QLASA study.
The two cases of ROXIE are probably one too much conservative, the other too much optimistic: in fact, it's true that the quench propagates from the outer to the inner layer in the high field turns at first, but then the transversal propagation is "helped" by the heat wave from the outer layer. So, the actual case is in the middle between the two approximations, and the QLASA simulations could be the more similar to it, because the quench is induced in the high field turns, then propagates in the transversal direction with a velocity higher than in ROXIE. This is probably due to the wrong magnetic field map: in a quadrupole there is a point in the coils where the magnetic field is zero, else in QLASA the magnetic field never goes to zero (see section 3.2.2), so the propagation is faster. In this case, this wrong approximation could be useful to simulate the actual case, in which the propagation is accelerated by the heat from the outer layer; however, the amount of this effect is not clear, so all these considerations can be considered valid only qualitatively.

4.3.6 Conclusions

The main consideration that can be made about all the study described in this section is that **the MQXF protection is very challenging**, under the assumptions made. The hot spot temperature are very close, and in some cases higher than the "conventional" upper safe designed limit of 350 K. The safe margin is therefore very little, and the uncertainties on the calculation (as material properties, true material fractions in the conductors, slower propagation from the outer to the inner layer, higher quench heaters delay time...) don't ensure that the protection is reliable. In addiction, eventual problems, as dumping failure or quench heaters breakage, could be dangerous for the magnet safety.
On the other hand, all the study has been performed considering the MQXF nominal inductance. We've seen in the chapter 3 that in both HQ and LQ during the current discharge the magnets had an effective inductance lower than the nominal one of $\sim 30\%$, because of some high dI/dt effects. So, all the estimations made in this section could be conservative, even if in MQXF the dI/dt is about 20 kA/s, against the 60 kA/s in HQ and LQ; however, it's impossible to give a quantitative estimation of the effect.
A very important protection feature is the quench heaters design: the design described in the section is not final, and eventual improvements could bring a better scenario for the protection.
Presently, a new version of the MQXF cable is going to be developed, and the protection will be updated.

Bibliography

[1] M. N. Wilson, *Superconducting magnets*. Mono. Cryog., Oxford: Clarendon Press, 1983.

[2] D.A. Edwards, M.J. Syphers, *An introduction to the Physics of High Energy Accelerators*. Wiley&Sons editors, 1993.

[3] L. Rossi and M. Sorbi, *QLASA: a computer code for quench simulation in adiabatic multicoil superconducting windings*. Tech. Rep. TC-04-13, INFN, 2004.

[4] N. Schwerg, H. Henke, and S. Russenschuck, *Numerical Calculation of Transient Field Effects in Quenching Superconducting Magnets*. PhD thesis, Berlin, Berlin, Tech. U., Berlin, 2009. Presented on 18 Nov 2009.

[5] S. Russenschuck, *Field Computation for Accelerator Magnets: Analytical and Numerical Methods for Electromagnetic Design and Optimization*. Weinheim: Wiley, 2010.

[6] G. Manfreda, L. Rossi, and M. Sorbi, *MATPRO upgraded version 2012: a computer library of material property at cryogenic temperature*. Tech. Rep. INFN-12-04/MI, INFN, April 2012.

[7] G. Ambrosio, N. Andreev, M. Anerella, E. Barzi, B. Bingham, D. Bocian, R. Bossert, S. Caspi, G. Chlachidize, D. Dietderich, J. Escallier, H. Felice, P. Ferracin, A. Ghosh, A. Godeke, R. Hafalia, R. Hannaford, G. Jochen, V. Kashikhin, M. J. Kim, P. Kovach, M. Lamm, A. McInturff, J. Muratore, F. Nobrega, I. Novitsky, D. Orris, E. Prebys, S. Prestemon, G. Sabbi, J. Schmalzle, C. Sylvester, M. Tartaglia, D. Turrioni, G. Velev, P. Wanderer, G. Whitson, and A. Zlobin, *Test results of the first 3.7 m long Nb3Sn quadrupole by LARP and future plans*. IEEE Transactions on Applied Superconductivity, vol. 21, no. 3, pp. 1858-1862, 2011.

[8] V. Marinozzi, *Guidelines for the quench analysis of Nb3Sn accelerator magnets using QLASA*. Tech. Rep. TD-13-008, Fermilab Technical Division, 2013.

[9] T. Salmi, *Modeling quench protection heaters in Nb3Sn accelerator magnets*. 2013. To be published at Proc. WAMSDO 2013.

[10] T. Salmi, *Protection heater delay time optimization in high-field Nb3Sn magnets*. 2013. To be submitted at MT23 conference.

[11] B.W. Robert, *Survey of superconductive materials and critical evaluation of selected properties*. J. Phys. Chem. Data, Vol.5, No.3, 1976.

[12] L.Rossi, *Study of the Superconductive-to-Resistive Transition for the US- LARP High Field Quadrupoles for the LHC Upgrade*. Bachelor degree thesis, Universitá degli Studi di Milano, 2012.

[13] G. Manfreda, G. Ambrosio, H. Felice, V. Marinozzi, T. Salmi, M. Sorbi, E. Todesco, G. Volpini, *Quench Protection Study of the Nb3Sn Low-β Quadrupole for the LHC Luminosity Upgrade*. 2013. To be submitted at MT23 conference.

[14] H. Felice, G. Ambrosio, M. Anerella, R. Bossert, S. Caspi, D. Cheng, D. Dietderich, P. Ferracin, A. K. Ghosh, R. Hafalia, C. R. Hannaford, V. Kashikhin, J. Schmalze, S. Prestemon, G.L. Sabbi, P.Wanderer, A.V. Zlobin, *Design of HQ - a High Field Large Bore Nb3Sn Quadrupole Magnet for LARP*. IEEE Transactions on Applied Superconductivity, Vol. 19, No.3, pp. 1235-1239, 2010.

[15] H. Bajas, G. Ambrosio, M. Anerella, M. Bajko, R. Bossert, S. Caspi, A. Chiuchiolo, G. Chlachidze, D. Dietderich, O. Dunkel, H. Felice, P. Ferracin, J. Feuvrier, L. Fiscarelli, A. Ghosh, C. Giloux, A. Godeke, A. R. Hafalia, M. Marchevsky, S. Russenschuck, G. L. Sabbi, T. Salmi, J. Schmalzle, E. Todesco, P. Wanderer, X. Wang, M. Yu, *Cold Test Results of the LARP HQ Nb3Sn quadrupole magnet at 1.9 K*. Presented at the Applied Superconductivity Conference, Portland, Oregon, USA, 2012.

[16] H. Felice, G. Ambrosio, M. D. Anerella, D. Bocian, R. Bossert, S. Caspi, B. Collins, D. Cheng, G. Chlachidze, D. R. Dietderich, P. Ferracin, A. Godeke, A. Ghosh, A. R. Hafalia, J. M. Joseph, J. Krishnan, M. Marchevsky, G. Sabbi, J. Schmalzle, P. Wanderer, X. R. Wang, and A. Zlobin, *Impact of Coil Compaction on Nb Sn LARP HQ Magnet*. IEEE Transactions on Applied Superconductivity, Vol. 22, 2012.

[17] M. Marchevsky, G. Ambrosio, B. Bingham, R. Bossert, S. Caspi, D. W. Cheng, G. Chlachidze, D. Dietderich, J. DiMarco, H. Felice, P. Ferracin, A. Ghosh, A. R. Hafalia, J. Joseph, J. Lizarazo, *Quench Performance of HQ01, a 120 mm Bore LARP Quadrupole for the LHC Upgrade*. IEEE Transactions on Applied Superconductivity, Vol. 22, No.3, 2012.

[18] M. Sorbi, *Studio della propagazione del quench e misure su avvolgimenti superconduttori adiabatici in $NbTi$ e Nb_3Sn*. Master degree thesis, Universitá degli Studi di Milano, 1993.

[19] L. Chiesa, *Quench protection analysis for the superconducting quadrupoles Q2a/Q2b for the inner triplet of LHC*. Master degree thesis, Universitá degli Studi di Milano, 2000.

[20] M. Canali, *Propagazione della transizione di fase superconduttiva-resistiva, termicamente indotta, in solenoidi multipli ad alti campi: studi e misure*. Master degree thesis, Universitá degli Studi di Milano, 1990.

Acknowledgments

First of all, I would like to thank my supervisor Dr. Massimo Sorbi. Thank you for the great opportunity that you gave me, for your constant help during my work, and for having trusted in my skills all the time.
Thanks to Dr. Giorgio Ambrosio. Thank you for having given me the opportunity to spent time at Fermilab, and for having helped me in all the situations that occurred in such a new, different place as the USA. This hard, and beautiful experience has been a good "gym" for my work and life journey.
Thanks to Ing. Giulio Manfreda. Thank you for having never, never, left anything without a good explanation. I wondered your interest in understanding so thoroughly the things, and it led me to learn much more.
Thanks to all the Fermilab TD staff, in particular to Guram and Mike. Thank you for all the time spent in hearing and helping me, despite your great amount of work.
At least, but not in importance, thanks to all my friends (it's impossible to nominate everyone!), to my family, and mostly to my girlfriend Ilaria. Thank you for your companionship, that is the greatest thing of my life.